Regd. No. C-3911

VOL. 35 **INDIAN JOURNAL OF PHYSICS** No. 4

(Published in collaboration with the Indian Physical Society)

AND

VOL. 44 **PROCEEDINGS** No. 4

OF THE

INDIAN ASSOCIATION FOR THE CULTIVATION OF SCIENCE

APRIL 1961

PUBLISHED BY THE

INDIAN ASSOCIATION FOR THE CULTIVATION OF SCIENCE

JADAVPUR, CALCUTTA 32

Annual Subscription—
Inland Rs. 25.00
Foreign £ 2-10-0 or $ 7.00

NOTICE
TO INTENDING AUTHORS

1. Manuscripts for publication should be sent to the Assistant Editor, Indian Journal of Physics, Jadavpur, Calcutta-32.

2. The manuscripts submitted must be type-written with double space on thick foolscap paper with sufficient margin on the left and at the top. The original copy, and not the carbon copy, should be submitted. Each paper must contain an Abstract at the beginning.

3. All References should be given in the text by quoting the surname of the author, followed by year of publication, *e.g.*, (Roy, 1958). The full Reference should be given in a list at the end, arranged alphabatically, as follows; Mazumder, M. 1959, *Ind. J. Phys.*, **33**, 346.

4. Line diagrams should be drawn on white Bristol board or tracing paper with black Indian ink, and letters and numbers inside the diagrams should be written neatly in capital type with Indian ink. The size of the diagrams submitted and the lettering inside should be large enough so that it is legible after reduction to one-third the original size. A simple style of lettering such as gothic, with its uniform line width and no serifs should be used, *e.g.*,

A·B·E·F·G·M·P·T·W·

5. Photographs submitted for publication should be printed on glossy paper with somewhat more contrast than that desired in the reproduction.

6. Captions to all figures should be typed in a separate sheet and attached at the end of the paper.

7. The mathematical expressions should be written carefully by hand. Care should be taken to distinguish between capital and small letters and superscripts and subscripts. Repetition of a complex expression should be avoided by representing it by a symbol. Greek letters and unusual symbols should be identified in the margin. Fractional exponents should be used instead of root signs.

NOTICE

No claims will be allowed for copies of journal lost in the mail or otherwise unless such claims are received within 4 months of the date of issue.

SCATTERING OF ELECTRON BY THOMAS-FERMI POTENTIAL

S. C. MUKHERJEE

Department of Theoretical Physics, Indian Association for the Cultivation of Science, Jadavpur, Calcutta-32

(*Received, February* 18, 1961)

ABSTRACT. In this paper the elastic scattering cross-section of electrons by the Thomas-Fermi potential as represented by the analytical forms due to Gombas and Tietz has been calculated by the Born approximation method. Our results are in fair agreement with those calculated with the exact numerical form of Thomas-Fermi potential. Further comparison shows that the Gombas-Tietz form is as good as those of Rozental and Buchdahl.

INTRODUCTION

The scattering of electron by a heavy atom is a many body problem, the electron to be scattered is influenced by the positively charged nucleus and the negatively charged electrons surrounding the nucleus. It is difficult to calculate accurately the electrical potential due to such an atom. Of the two available methods, the self-consistent field method of Hartree and Fock is more accurate than the statistical one of Thomas and Fermi. The difficulty of calculation by Hartree's method increases with the complexity of the atom, whereas the more complex the atom is the more valid is the calculation for the Thomas-Fermi potential, because the electrons of the complex atom are treated as a statistical emsemble. The form of the Thomas-Fermi potential is taken to be

$$V(r) = -\frac{Ze^2}{r}\phi(x)$$

where ϕ is the Thomas-Fermi function for the free neutral atom and is the solution of

$$\frac{\partial^2\phi}{\partial x^2} = \frac{\phi^{3/2}}{x^{\frac{1}{2}}}$$

where $x = r/\mu$; $\mu = \dfrac{0.88534}{Z^{1/3}}\, a_0$, a_0 being the first Bohr radius and Z is the atomic number. The above equation does not admit of an exact solution which is available only in the form of a numerical table ; however, various approximations in analytical forms have been suggested by several authors like Sommerfeld (1932), Rozental (1935), Gombas (1949), March (1950), Kerner (1951), Tietz

(1955, 1956), Brinkman (1954), Umeda (1955), Buchdahl (1956) and Latter (1955). It is not possible to calculate analytically the scattering cross section with the forms of Sommerfeld, March, Umeda and Latter. The form of Kerner is not quite suitable. Majewasky and Tietz (1957) have calculated scattering cross section in the Born approximation with the forms of Brinkman, Buchdahl and Rozental. The form of Gombas (1949) is valid only in a region near the nucleus and that of Tietz (1954) holds good outside this region. We propose to calculate the scattering cross section with the Gombas-Tietz form. We are led to this choice of the potential, because Tsang (1959) taking the form of Gombas has got good agreement of binding energies of electrons with those obtained by using the Thomas-Fermi potential and by Hartree's method. In this paper we have calculated by the Born approximation method the elastic scattering cross section of electrons by a central potential which is of the form of Gombas between the range $0 \leqslant x \leqslant 1$ and of Tietz for $x \geqslant 1$. We have compared our findings obtained by such a potential with the results of Mott and Massey (1949) obtained with Thomas-Fermi potential and that of Tietz and Majewasky (1957) calculated with the potentials of Rozental (1935) and Buchdahl (1956).

For electrons having 50 KeV energy scattered by Krypton ($Z=36$) the differential cross section decreases with increasing angle upto 70° ; thereafter it fluctuates with two maxima at 80° and 110°. Unfortunately there is no experimental data to compare with our theoretical findings.

CALCULATION

The amplitude of scattering by a central potential $V(r)$, according to the Born approximation, is given by

$$f(\theta) = -\frac{8\pi^2 m}{h^2} \int_0^\infty \frac{\sin kr}{kr} V(r) r^2 dr \qquad \ldots (1)$$

where θ is the scattering angle,

$$K = k|\, n_0 - n \,| = \frac{4\pi \sin \theta/2}{\lambda} \; ; \; \lambda = \frac{2\pi}{k} = \frac{h}{mv}$$

n_0 being the unit vector along the Z-axis, n is a unit vector along the direction of r.

In the case of scattering of electrons by an atom we choose the potential as

$$V(r) = V_G \quad \text{valid for } 0 \leqslant x \leqslant 1 \qquad \ldots (2)$$

$$= V_T \quad \text{valid for } x \geqslant 1$$

where V_G has the form as given by Gombas,

$$V_G = -\frac{Ze^2}{x\mu}\{0.878-0.546x+0.415(x-0.5)^2\}$$

where $x = \frac{r}{\mu}$; $\mu = \frac{0.88534}{Z^{1/3}}\ a_0$, and a_0 being the first Bohr radius for hydrogen and Z is the atomic number, and the form of V_T is due to Tietz,

$$V_T = -\frac{Ze^2}{x\mu}\left\{\frac{a^2}{(x+a)^2}\right\}$$

where $a = 1.86$, the values of x and μ are the same as in V_G. Substituting the form of (2) in Eq. (1), we get

$$f(\theta) = -\frac{8\pi^2 m\mu^3}{h^2 p}\left\{\int_0^1 \sin px\ V_G x dx + \int_1^\infty \sin px\ V_T x dx\right.$$

where

$$p = 2\mu k \sin\theta/2 = K\mu$$

$$K = 2k \sin\theta/2.$$

$$\therefore \quad \frac{f(\theta)}{Z^{1/3}} = \frac{83.07\times10^{-10}}{p}\left[\sin p\left(-\frac{0.131}{p^2}\right) + \cos p\left(\frac{0.830}{p^3} - \frac{0.435}{p}\right)\right.$$

$$+\frac{0.981}{p} - \frac{0.830}{p^3} + a^2\left\{\frac{\sin p}{1+a} - p\left(\cos pa\ Ci\{p(1+a)\} + \sin pa\ Si\{p(1+a)\}\right.\right.$$

$$\left.\left.\left.-\sin pa\ \frac{\pi}{2}\right)\right\}\right]$$

where $$Si(x) = \int_0^x \frac{\sin t}{t}\,dt\ ;\ Ci(x) = -\int_x^\infty \frac{\cos t}{t}\,dt$$

For the sake of comparison we give also the results of Tietz and Majewasky (1957) who have calculated the same with the potential forms of Rozental and Buchdahl.

The Rozental form is as follows :

$$\phi(x) = \sum_{i=1}^{3} C_i\, e^{-a_i x}$$

where C_i and a_i are constants and their values are $c_1 = 0.255$, $c_2 = 0.581$, $c_3 = 0.164$, $a_1 = 0.246$, $a_2 = 0.947$, $a_3 = 4.356$.

The Buchdahl form is as follows :

$$\phi(x) = [(1+Ax)(1+Bx)(1+Cx)]^{-1}$$

where $A = 0.9288$, $B = 0.1536$, $C = 0.05727$.

TABLE I

Comparison of our results for $|f(\theta)|^2$ with the numerical results of Mott and Massey and results of Rezental and Buchdahl

	$\|f(\theta)\|^2 Z^{-2/3}$ in units of 10^{-18}cm^2			
$p=2\mu K \sin\theta/2$	Mott & Massey	Rozental	Buchdahl	Present author
0.1	1460	1525	1257	1296
0.2	678	654	690	642
1.0	18.7	17.1	21.2	20.79
2.0	2.52	2.49	2.45	2.74
5.0	0.089	0.096	0.091	0.094
6.0	0.047	0.048	0.046	0.051
8.0	0.016	0.016	0.017	0.016
10.0	0.0064	0.0063	0.0065	0.0057

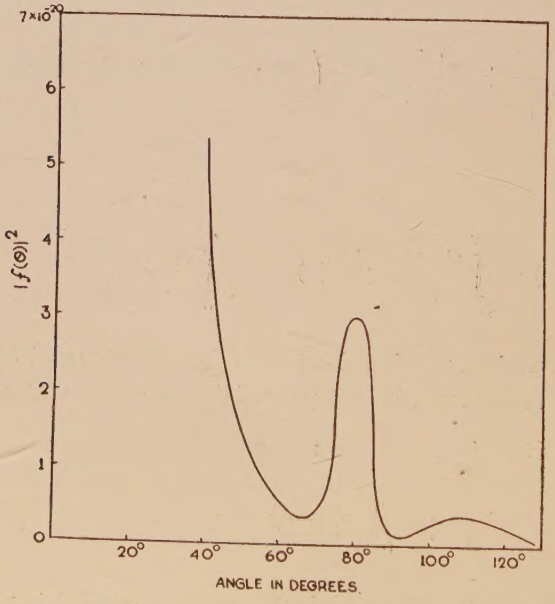

Fig. 1. Angular distribution of electrons at 40 KeV scattered by krypton (z=36)

DISCUSSION

From the table of comparison it appears that our result of differential scattering cross section calculated with the Gombas-Tietz form agrees pretty well with the results of Mott and Massey. Our results are as good as those calculated with the forms of Rozental and Buchdahl.

From the calculation it is found that when p is large the contribution to the scattering from the Gombas potential is much larger than that from the Tietz potential whereas when p is small the reverse is the case. This finding is in conformity with the physical picture; the larger the value of p is, greater is the number of particles coming under the influence of Gombas part of the potential.

For 50 KeV electrons scattered by Krypton ($Z = 36$) the differential cross section decreases with increasing angle till 70°, after which there are small rise and fall of the values giving two maxima which are analogous to diffraction phenomenon.

ACKNOWLEDGMENT

The author is grateful to Prof. D. Basu for suggesting the problem and for his constant guidance throughout the progress of this work.

7

REFERENCES

Brinkman, H. C., 1954, *Physica* **20**, 44.
Buchdahl, H. A., 1956, *Ann. Physik* **17**, 238.
Gombas, P., 1949, Die Statitische Theorie des Atoms und Thre Anwendungen (Springer-Verlag).
Kerner, E. H., 1951, *Phys, Rev.*, **83**, 71.
Latter, R., 1955, *Phys. Rev.* **99**, 510.
March, N. H., 1950, *Proc. Cambridge Phil. Soc.* **46**, 356.
Mott, N. F., & Massey, H. S. W., The Theory of Atomic Collisions (Oxford University Press, New York, 1949, Second Edition, Ch. IX).
Rozental, S., 1935, *Z. Physik*, **98**, 742.
Sommerfeld, A., 1932, *Z. Physik*, **78**, 283.
Tietz, T., 1955, *J. Chem. Phys.* **23**, 1167.
Tietz, T., 1956, *Nuovo Cimento* **4**, 1192 (1956).
Tietz, T. & Majewasky, M., 1957, *Phys. Rev.* **108**, 193.
Tsang, T., 1959, *Physica*, **25**, 1241.
Umeda, K., 1955, *J. Phys. Soc. Japan*, **10**, 749.

19

A SIMPLE STUDY OF THE NUCLEAR SELF-CONSISTENT FIELD PROBLEM*

N. V. V. J. SWAMY

Department of Physics, Karnatak University, Dharwar

(*Received, October* 10, 1960)

ABSTRACT. Assuming a nucleon-nucleus potential and a phenomenological nucleon density distribution, a Hartree type self-consistent field calculation has been carried out for O^{16}. Three cycles have indicated that the nucleus collapses in each cycle if only a pure central attraction of the Yukawa type is assumed to exist between the nucleons. Introduction of a repulsive core, other than the usual hard sphere type, has led to the conclusion that angular momentum dependent potentials have to be used in order to obtain convergence in successive cycles and adequate binding energy of the nucleus. An estimate has been made of the correlation length of the resulting non-local potential, as also of the effective mass as a function of position.

There can be no question that the many-body approach of Brueckner and Bethe (1955, 1956) is the correct one for studying the nuclear self-consistent field problem. However it has been noticed that the application of this method to finite nuclei bristles with outstanding computational difficulties. It is the purpose of this paper to point out that when a Hartree type self-consistent field calculation has been carried out based on a single-particle approach, the qualitative results so obtained did not differ in physical content very much from those of the many body theory.

The earlier effort in this direction has been that of Talman (1956) who had chosen a two-body interaction of the Yukawa type between all pairs of nucleons

$$\vec{G}(\vec{r}_1,\vec{r}_2) = g^2 \frac{e^{-p|\vec{r}_1-\vec{r}_2|}}{|\vec{r}_1-\vec{r}_2|} \qquad \ldots (1)$$

g being the coupling constant or strength of the two-body force and p^{-1} the range of the force. Using a uniform nucleon density distribution

$$\vec{\rho}(r) = \rho(r) = \frac{3A}{4\pi a^3} \qquad r<a$$

$$= 0 \qquad r>a \qquad \ldots (2)$$

*Work supported by the United States Atomic Energy Commission. This work was performed when the author was at the Florida State University, Tallahassee, Florida. A summary of the results reported herein was included in a lecture given by the author at the First Summer School in Theoretical Physics held at Mussoorie during May–June 1959.

the nucleon-nucleus potential was computed in accordance with

$$\vec{V(r_1)} = \int \vec{G(r_1,r_2)}\vec{\rho(r_2)}\vec{dr_2} \qquad \ldots \quad (3)$$

With this potential Talman has solved the Schrodinger equation numerically and from the wave functions thus obtained a new density distribution was computed which in turn gave a potential in accordance with Eq. (3) above. Proceeding in this manner he found that, at the end of one complete cycle of calculation, the nucleus collapsed and the total energy of a system of 150 nucleons was low, yielding a binding energy per particle of about ·94 MeV.

It is not sufficient if self-consistency is achieved between a nuclear potential and any density, but the density should be in agreement with experiment. The Levy (1953) potentials for instance show saturation but not at true density. The uniform density used by Talman is rather unrealistic from a phenomenological point of view. We have, therefore, attempted to ascertain the results of successive cycles in a self-consistent field calculation using phenomenological densities given by Green (1956), which have the virtue of close agreement with the Stanford charge distributions. The density distribution obtained by Green of nucleons moving in a square well with an exponentially diffuse boundary, involves Bessel functions of exponential functions. Therefore, in their original form, the wave functions are too complicated to handle. Choosing a closed-shell light nucleus of O^{16}, the nodeless s and p radial wave functions have been approximated (Swamy 1958) by Slater type functions :

$$\begin{aligned} R_{1s} &= 1{\cdot}764 r^{1{\cdot}429} e^{-1{\cdot}318r} \\ R_{1p} &= 1{\cdot}122 r^{3{\cdot}195} e^{-1{\cdot}737r} \end{aligned} \qquad \ldots \quad (4)$$

For simplicity in an initial effort, Coulomb, exchange and tensor forces were neglected. Assuming a purely direct and central interaction between any two nucleons, of the form given in Eq. (1), the zero stage potential was calculated by means of Eq. (3) where in the integrand the approximate phenomenological density was used. The multiplying constant in Eq. (1) has been chosen such that the nucleon-nucleus potential 'strength' matches that of the square well with exponentially diffuse boundary. The two-body force range was chosen, as an experiment, to be 1·144 fermis.

As in the Hartree method, the potential felt by any one particle is obtained by subtracting its own contribution from the total nuclear potential. The second phase of the self-consistent field treatment is to secure a new nucleon density by solving the Schrodinger equation for each single particle state with the potential thus obtained. All the particles in the nucleus chosen being in their ground states, a variational method has been used to solve the Schrodinger equation approximately. This method has the advantage of being speedier than

a numerical solution of the differential equation and is fairly reasonable for forming a qualitative estimate of the trend of affairs as we go through successive cycles. In the detail of the variational calculation a scale factor multiplying the radial coordinate has been used as the variational parameter (Hartree, 1955). The trial function used was

$$\phi_e = \sqrt{\lambda}\, R_{1e}(\lambda r) \qquad \ldots \quad (5)$$

the variational parameter being λ. With the help of the wave functions thus obtained the expectation values of the potential and kinetic energy operators have also been calculated in order to know the total binding energy of the nucleus. Further going back to Eq. (3) a second stage potential has been computed and the cycle was set going once again. The results of three full cycles of such calculations have been that

(a) the nucleus shrinks in each cycle, though not too rapidly and the potential becomes more diffuse in each cycle;

(b) the energy eigenvalue of a single particle state increases in each cycle, though perhaps slightly;

(c) the total energy of the system is positive in sign and becomes increasingly positive in each cycle thus giving no binding at all.

These results are shown in Table I. With a view to ascertaining the sensitiveness of the rate of collapse to the two body force range, a different two body force range has been chosen and the calculations repeated. Table II shows that this sensitiveness is considerable.

TABLE I

Results of two successive cycles showing shrinkage of nucleus

	Zero stage	End of I cycle	End of II cycle
Mean square radius of potential in fermi (Bruecner *et al.*, 1955)	15.305	14.944	14.469
Expectation of kinetic energy operator for s state $\langle T_s \rangle$ in MeV	11.726	12.772	13.793
–do– for p state $\langle T_p \rangle$	18.239	19.522	20.939
Expectation of potential energy operator for s state $\langle V \rangle_s$ in MeV	−35.367	−37.865	−40.966
–do– for p state $\langle V \rangle_p$	−28.099	−30.163	−32.601
Energy eigen value of s state in MeV W_s	−23.641	−25.093	−27.173
–do– for p state W_p	− 9.860	−10.641	−11.662
Total binding energy in MeV	+26.444	+28.648	+28.908

TABLE II

Two body force range in fermi	Mean square radius of potential in fermi (Brueckner *et al.*, 1958)	
1.143	15.305	Zero stage
	14.944	End of I Cycle
	14.469	End of II Cycle
0.500	8.943	Zero Stage
	6.418	End of I Cycle
	5.585	End of II Cycle

With a purely attractive two body interaction, therefore, it has not been possible to achieve stability and convergence in successive cycles of the self-consistent field calculation. Now it has been fairly well known that exchange plus a repulsive core ensures saturation. A repulsive term was therefore introduced into the two body interaction as the next logical step in the study. The repulsive cores that exist in the literature consist of hard sphere interactions at a distance of ·4 or ·5 fermis between two nucleons. Introduction of such a core in $G(\vec{r}_1,\vec{r}_2)$ would make the integral in Eq. (3) singular, unless some cut-off device is introduced. As an alternative, however, a form of interaction is assumed which would give a very large repulsion at short distances and becomes infinite only when the two nucleons collide. A Green's function of the following form containing an integrable singularity will ensure this behaviour :

$$G(\vec{r}_1,\vec{r}_2) = -g_A{}^2 \frac{e^{-p_A|\vec{r}_1-\vec{r}_2|}}{|\vec{r}_1,-\vec{r}_2|} + g_R{}^2 \frac{e^{-p_R|\vec{r}_1-\vec{r}_2|}}{|\vec{r}_1-\vec{r}_2|} \quad \ldots \quad (6)$$

Here the subscripts A and R stand for attraction and repulsion respectively. It is interesting to note that such a Green's function does arise out of a non-linear meson theory (Green, 1949). The effect of introducing such a repulsion has been studied in two ways —(a) the coupling constant of the repulsive term g_R is varied keeping other things constant, (b) keeping the coupling constant fixed, the range of repulsion $p_R{}^{-1}$ is varied. In both cases the attractive force range is 1·144 fermis and the attractive coupling constant 35·543 MeV. The zero stage values of $<r^2>$ of the s and p orbitals are respectively 5·780 and 8·084 fermi (Brueckner *et al.*, 1955). The results are shown in Table III. It can be seen from this that either there is no convergence in successive cycles (nucleus collapsing in each cycle) or where there is an approach to convergence, the total binding energy becomes much too small. It has thus not been possible to choose one set of four parameters g_A, $p_A{}^{-1}$, g_R, $p_R{}^{-1}$ in order to meet the dual requirements

of stability and covergence in successive cycles as well as obtaining the experimental total binding energy of the nucleus. On the other hand, an approach which has proved to be a successful way out of this difficulty is that of choosing different coupling constants for the two angular momentum states viz., s and p states. The following set of parameters have been effective in indicating convergence in successive cycles, as well as yielding a total binding energy of 124·34 MeV.

s state $g_A^2 = 2177{\cdot}5e^2$ $g_R^2 = 8912{\cdot}9e^2$ $p_A^{-1} = 1{\cdot}414$ fermis $p_R^{-1} = {\cdot}143$ fermis

p state $g_A^2 = 2177{\cdot}5e^2$ $g_R^2 = 9333{\cdot}1e^2$ $p_A^{-1} = 1{\cdot}414$ fermis $p_R^{-1} = {\cdot}143$ fermis

e = charge of an electron

TABLE III

Effect of repulsive term in the two body interaction

g_R^2 in MeV	35.543	35.543	35.543	7.109	25.543	71.087
P_R^{-1} in fermi	0.500	0.667	1.000	0.500	0.500	0.500
			s state			
$\langle r^2 \rangle$ in fermi (Brueckner, *et al.*, 1955)	4.007	4.381	4.822	3.742	4.007	4.147
W_s in MeV	−49.300	−42.866	−28.903	−57.460	−49.300	−39.310
$\langle T_s \rangle$ in MeV	14.366	13.143	11.395	15.395	14.366	13.889
$\langle V \rangle_s$ in MeV	−63.666	−56.009	−40.838	−72.855	−63.666	−53.197
Contribution to total binding per particle in MeV	−17.467	−14.862	− 8.404	−21.032	−17.467	−12.711
			p state			
$\langle r^2 \rangle$ in fermi	5.681	6.603	7.429	4.922	5.681	6.141
W_p in MeV	−32.526	−26.856	−14.654	−41.059	−32.526	−23.241
$\langle T_p \rangle$ in MeV	25.065	21.573	19.184	28.961	25.065	23.206
$\langle V \rangle_p$ in MeV	−57.590	−48.429	−32.838	−70.025	−57.590	−46.452
Contribution to total binding per particle in MeV	−3.731	−2.641	+2.265	−6.047	−3.731	−0.200

The parameters of the attractive term are taken from Gammel (1957). It is clear, of course, that because of the rather crude method used in solving the Schrodinger equation the numerical figures arrived at constitute no more than

an indication of the trend of affairs leading to the important conclusion that the nucleon-nucleus potential turns out to be angular momentum dependent or momentum dependent in general.

Momentum dependent potentials can, in coordinate space, be represented by a non-local potential i.e., a potential matrix (Bethe, 1956). The Schrodinger equation for the relative motion of a nucleon in this potential is

$$\frac{\hbar^2}{2M}\Delta^2\vec{\psi_e}(r)+E_e\vec{\psi_e}(r)=\int\vec{(r^1}\mid V\mid\vec{r})\vec{\psi_e}(r^1)\vec{dr^1} \qquad \ldots (7)$$

Comparing this with the following equation which is satisfied by the potentials discussed above

$$\frac{\hbar^2}{2M}\Delta^2\vec{\psi_e}(r)+E_e\vec{\psi_e}(r)= V_e\vec{\psi_e}(r) \qquad \ldots (8)$$

we readily get the relation

$$V_e(\vec{r})\vec{\psi_e}(r)=\int\vec{(r^1}\mid V\mid\vec{r})\vec{\psi_e}(r^1)\vec{dr^1} \qquad \ldots (9)$$

Following Frahn and Lemmer (1957) we have assumed that

$$\vec{(r^1}\mid V\mid\vec{r})=\frac{V\left(\frac{\vec{r}+\vec{r^1}}{2}\right)e^{\frac{-(\vec{r}-\vec{r^1})^2}{a_c^2}}}{\pi^{3/2}a_c^3} \qquad \ldots (10)$$

where a_c is a 'non-locality parameter' or 'correlation length'. This correlation length has been estimated to be 1·1 fermis. In the effective mass approximation, the equation of motion of a particle in a momentum dependent potential well is replaced by one describing the motion in a static well, but having a variable mass which now becomes function of position. In this case the kinetic energy operators have to operate on the mass and, in order to meet the requirement of Hermiticity and relavistic invariance, have to be properly symmetrized. Frahn and Lemmer (1957) have shown that the appropriate Schrodinger equation is

$$\frac{-\hbar^2}{8}\left[\Delta^2\frac{1}{M(r)}+\Delta\frac{2}{M(r)}\Delta+\frac{1}{M(r)}\Delta^2\right]\vec{\psi(r)}+\vec{V(r)}\vec{\psi(r)}=E\vec{\psi(r)} \qquad \ldots (11)$$

where the effective mass $M(r)$ is related to the actual mass M through the local potential $V(r)$ by

$$M(r)=\frac{M}{1-\frac{a_e^2 M\ V(r)}{2\hbar^2}} \qquad \ldots (12)$$

Using Eqns. (6), (3), (9), (10) and the radial part of Eq. (11) the equivalent $V(r)$ and hence $M(r)$ in Eq. (12) have been calculated. The latter is shown in Fig. 1.

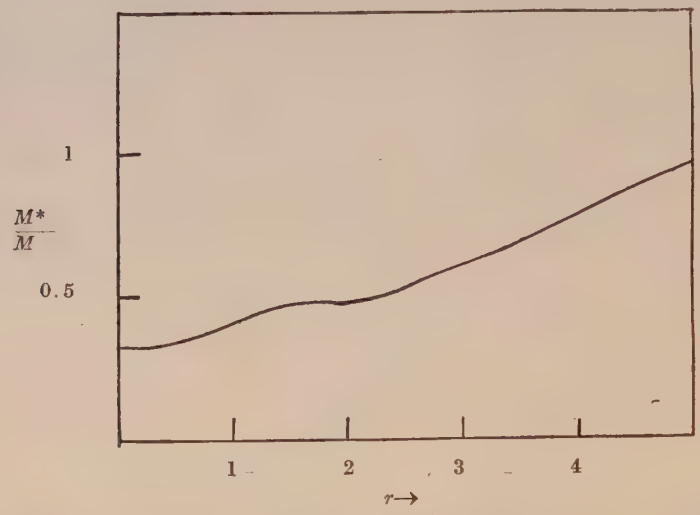

Fig. 1. Spatial variation of effective mass. M is the true nucleon mass.

In conclusion we have to state that, while the calculations do not have the certainty of accuracy because of the approximations used, the results arrived at through a simple single-particle approach do agree with the more fundamentally thorough many-particle approach.

It is a pleasure to acknowledge the interest and constant guidance received from Dr. Alex E. S. Green during the course of this work. The financial assistance of the U.S. Atomic Energy Commission is gratefully acknowledged.

REFERENCES

Bethe, H. A., 1956, *Phys. Rev.*, **103**, 1353.
Brueckner, K. A. and Levinson, C. A., 1955, *Phys. Rev.*, **97**, 1344.
Frahn, W. E., and Lemmer, R. H., 1957, *Nuovo Cimento*, **5**, 1564.
Gammel, J. L., Christian, R. S., and Thaler, R. M., 1957, *Phys. Rev.*, **105**, 311.
Green, A. E. S., 1948, *Phys. Rev.*, **73**, 26.
Green, A. E. S., Lee, K., and Berkeley, R., 1956, *Phys. Rev.*, **104**, 1625.
Hartree, D. R., Douglas, A. S. and Runciman, W. A., 1955, *Proc. Cam. Phil. Soc.*, **51**, 486.
Levy, M. M., 1953, *Phys. Rev.*, **88**, 575.
Swamy, N. V. V. J., Ph.D. Thesis (unpublished), 1958.
Talman, J. D., 1956, *Phys. Rev.*, **102**, 455.

20

POTENTIAL CONSTANTS AND CALCULATED THERMODYNAMIC PROPERTIES OF NITRYL FLUORIDE AND NITRYL CHLORIDE

P. G. PURANIK AND E. V. RAO

DEPARTMENT OF PHYSICS, UNIVERSITY COLLEGE OF SCIENCE,
OSMANIA UNIVERSITY, HYDERABAD 7. (A.P.)

(*Received, January* 7, 1961)

ABSTRACT. Using a most general quadratic potential energy expression the molecule NO_2R, where R is either F or Cl, is subjected to normal coordinate treatment. Two sets of thirteen force constants for each molecule have been proposed, and the fundamental frequencies have been calculated with the help of Wilson's F-G matrix method. The calculated and the observed values of the frequencies closely agree. Thermodynamic properties for the fluoride and the chloride have been calculated for temperatures in the range of 100-1000 °K.

1. INTRODUCTION

The infrared and Raman spectra of nitryl fluoride are reported by Rolfe and Woodward (1956) and that of nitryl chloride have been studied by Ryason and Wilson (1954). The latter authors have assigned the frequencies of the chloride molecule. Assuming the valence force potential function Hariharan (1958) has used the observed values of the frequencies and calculated the force constants by using Wilson's F-G matrix method and assigned the fundamental frequencies of both the molecules. His assignments differ from those of Ryason and Wilson so far as frequencies 651 and 411 cm^{-1} are concerned. Ryason and Wilson have assigned 651 cm^{-1} to class A_1 and 411 cm^{-1} to class B_2, whereas Hariharan has reversed the assignments. Hariharan has neglected most of the interaction force constants and his value for f_α in the case of nitryl fluoride is negative which cannot be justified.

With a view to checking the earlier assignments the authors, using a most general quadratic potential energy expression, and assuming a planar configuration for the molecules and the point group C_{2v}, have carried out normal coordinate treat- ment, according to Wilson's $F-G$ matrix method.

II. NORMAL COORDINATE TREATMENT

The planar configuration of NO_2R where R can be either F or Cl has a symmetry of C_{2v} point group ($3A_1$, $2B_2$, B_2). The symbols used for the equilibrium values of bond distances and interbond angles are shown in Fig. 1.

The examples of possible types of potential constants arising out of various types of interactions are given below.

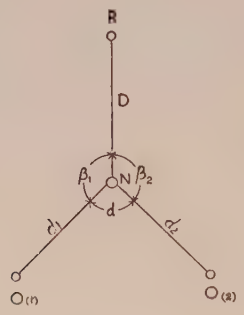

Fig. 1.

f_d = N-O stretching constant.

f_α = <O-N-O bending constant.

$f_\beta{}^\beta$ = <R-N-O(1) and <R-N-O(2) angle angle interaction constant.

$f_d{}^d$ = N-O(1) and N-O(2) bond bond interaction constant.

$f'_d{}^\beta$ = N-O(1) and <R-N-O(2) bond angle interaction constant.

The most general quadratic expression for potential energy is

$$2V = f_D(\Delta D)^2+f_d\{(\Delta d_1)^2+(\Delta d_2)^2\}+d^2f_\alpha(\Delta\alpha)^2+d^2f_\beta\{(\Delta\beta_1)^2+(\Delta\beta_2)^2\}+2f_d{}^d\Delta d_1\Delta d_2+$$
$$+2f_D{}^d\Delta D(\Delta d_1+\Delta d_2)+2df_D{}^\alpha\Delta D\Delta\alpha+2df_d{}^\beta\Delta d(\Delta\beta_1+\Delta\beta_2)+2df_d{}^\alpha(\Delta d_1+\Delta d_2)\Delta\alpha$$
$$+2d^2f_\alpha{}^\beta\Delta\alpha(\Delta\beta_1+\Delta\beta_2)+2d^2f_\beta{}^\beta\Delta\beta_1\Delta\beta_2+2df_D{}^\beta\Delta D(\Delta\beta_1+\Delta\beta_2).$$

The symmetry coordinates for A_1 type of vibrations are :

$R_1 = \Delta D.$

$R_2 = 1/\sqrt{2}(\Delta d_1+\Delta d_2).$

$R_3 = 1/\sqrt{6}(2\Delta\alpha-\Delta\beta_1-\Delta\beta_2).$

$R_4 = 1/\sqrt{3}(\Delta\alpha+\Delta\beta_1+\Delta\beta_2) \equiv 0$ (Redundant).

For B_1 type :-

$R_5 = 1/\sqrt{2}(\Delta d_1-\Delta d_2).$

$R_6 = 1/\sqrt{2}(\Delta\beta_1-\Delta\beta_2).$

For type B_2 (Out of plane)

$R_7 = d\Delta\gamma.$

The symmetry coordinates are normalized and orthogonal. From the potential energy matrix i.e. '*f*' matrix and the matrix formed by the coefficients

contained in the symmetry coordinated the following '*F*' matrix elements are obtained.

The '*F*' matrix elements are

For type A_1

$F_{11} = f_D$

$F_{12} = \sqrt{2} f_D{}^d$.

$F_{13} = \sqrt{(2/3)} d(f_D{}^\alpha - f_D{}^\beta)$.

$F_{22} = f_d + f_d{}^d$.

$F_{23} = 1/\sqrt{3} d(2f_d{}^\alpha - f_d{}^\beta - f_d{}'^\beta)$.

$F_{33} = 1/3d^2(2f_\alpha + f_\beta + f_\beta{}^\beta - 4f_\alpha{}^\beta)$.

For the type B_1.

$F_{11} = f_d - f_d{}^d$.

$F_{12} = d(f_d{}^\beta - f_d{}'^\beta)$.

$F_{22} = d^2(f_\beta - f_\beta{}^\beta)$.

For the type B_2.

$F_{11} = f_\gamma$.

Elements of G matrices* obtained with the help of Decius Tables (1948) are as follows.

For the type A_1.

$G_{11} = \mu_N + \mu_R$.

$G_{12} = \sqrt{2}\mu_N \cos\beta$.

$$G_{13} = \sqrt{(2/3)} a\mu_N \left\{ \sin\beta - \frac{2\cos\beta}{\sin\alpha}(1-\cos\alpha) \right\}$$

$G_{22} = \mu_0 + \mu_N(1+\cos\alpha)$

$$G_{23} = \mu_N/\sqrt{3} \left[\frac{1}{\sin\beta}(a - b\cos\beta)\cos\beta + (b - a\cos\beta)(1+\cos\alpha) - 2a\sin\alpha \right]$$

$G_{33} = 1/3[4a^2\{\mu_0 + \mu_N(1-\cos\alpha)\} + b^2\mu_R + a^2\mu_0 + \mu_N(a^2 + b^2 - 2ab\cos\beta)$

$+ b^2\mu_R y + \mu_N\{(b - 2a\cos\beta)by\} + a^2\{\sin^2\beta(1-y^2) + y\cos\alpha)\}$

$-4\mu_0 a^2 x - 4\{(a - a\cos\alpha - b\cos\beta)ax + (\sin\alpha\sin\beta(1-x^2) + x\cos\beta)ab\}\mu_N]$.

For type B_1.

$G_{11} = \mu_0 + \mu_N(1\text{-}\cos\alpha)$.

$G_{12} = -(\mu_N/\sin\beta)(b - a\cos\beta)(1-\cos\alpha)$.

$G_{22} = (\mu_R/\sin^2\beta)b^2(1-\cos\alpha) + \mu_0 a^2 + (\mu_N/\sin^2\beta)(b - a\cos\beta)^2(1-\cos\alpha)$.

For type B_2.

$$G_{11} = (1/2)\mu_0 \cos^2\beta + \mu_N \frac{(D - d\cos^2\beta)}{D^2\cos^2\beta} + \mu_R d^2/D^2.$$

In the above expressions

$$a = 1/d, \text{ and } b = 1/D$$
$$x = (\cos\beta - \cos\alpha\cos\beta)/\sin\alpha\sin\beta.$$
$$y = (\cos\alpha - \cos^2\beta)/\sin^2\beta.$$

For calculating the g matrix elements the values of bond distances, bond-bond angles and the masses of different atoms are taken from Table I (1958).

TABLE I

Bond distances, interbond angles, masses of different atoms, and moments of inertia of nitryl fluoride and nitryl chloride

	Bond distances		
	$F\text{-}NO_2$	$Cl\text{-}No_2$	Mass of the atom.
N-O (d)	1.22 A	1.16 A	m_0 = 16.00 (a.w.u.)
N-R (D)	1.50 A	1.98 A	m_N = 14.008 (a.w.u.)
			m_{61} = 35.457 (a.w.u.)
			m_F = 19.000 (a.w.u.)
	Interbond angles		Moments Of Inertia.
<O-N-O (α)	150°	130°	I_x^F = 40.7369, I_y^F = 44.436, I_z^F 85.173.
<R-N-O (β)	105°	115°	I_x^{Cl} = 110.212, I_y^{Cl} = 35.367, I_z^{Cl} = 145.579

Note :—The symmetry number for this form is 2.
The moments of inertia are given in units of (a.w.u.A^2).

In the first calculations the force constants derived by Hariharan were used in toto and interaction constants which he has ignored, were proposed by the authors, keeping in view the proper order of the magnitude of such force constants. After a few modifications the observed frequencies were reproduced by calculations with an error within one per cent. The force constants finally proposed by the authors are given in Table II. The six corresponding force constants derived by Hariharan are given for comparison.

The observed and the calculated values of the in-plane fundamental vibrational frequencies of both the molecules are given in Table III. The aggreement between the observed and the calculated values is a check on the probable accuracy of the force constants proposed.

III. THERMODYNAMIC PROPERTIES

The heat capacity C°_p, heat content $(H_0 - E_0^0)/T$ free energy $-(F_0 - E_0^0)/T$ and entropy S° at constant pressure for both the molecules with a rigid rotator and harmonic oscillator approximation for the ideal gaseous state at one atmos-

pheric pressure were calculated for twelve temperatures in 100—1000°K range. The results are given in Tables IV and V.

TABLE II

Potential constants for nitryl fluoride and nitryl chloride

Pot. Constants	Nitryl fluoride		Nitryl chloride	
	Authors	Hariharan	Authors	Hariharan
f_d	12.3	10.86	10.25	9.48
f_D	3.3	3.51	4.19	4.19
$f_d{}^d$	2.7	2.04	0.95	0.52
$f_D{}^d$	1.5	—	1.0	1.41
f_β	1.10	1.13	0.59	0.62
$f_\beta{}^d$	0.48	—	0.30	—
$f^\alpha{}_d$	0.40	—	0.25	—
$f_D{}^\beta$	0.30	—	0.20	—
f_α	0.15	–0.13	0.35	0.36
$f_d{}'{}^\beta$	0.12	—	0.10	—
$f_D{}^\alpha$	0.10	—	0.06	—
$f_\alpha\beta$	0.06	—	0.02	—
$f_\beta\beta$	0.05	—	0.03	—

Note :—Bond constants and bond-bond interactions constants are given in md/A, bond-angle interaction constants in md/rad, and angle constants and angle-angle interaction constants are given in mdA/rad^2.

TABLE III

Observed and calculated values of the fundamental frequencies of nitryl fluoride and nitryl chloride

Type	Nitryl fluoride		Nitryl Chloride	
	Observed	Calculated	Observed	calculated
$A_1(\nu_1)$	1312	1312	1293	1296
$A_1(\nu_2)$	822	828	794	798
$A_1(\nu_3)$	460	459	411	404
$B_1(\nu_4)$	1793	1791	1685	1683
$B_1(\nu_5)$	570	567	367	360

TABLE IV

Heat capacity, heat content, free energy and entropy for nitryl fluoride

Temp. (K)	C_p^0	$(H_0\text{-}E_0^0)/T$	$-(F_0\text{-}E_0^0)/T$	S^0
100	8.11	7.97	43.90	51.87
200	9.86	8.42	49.52	57.95
273	11.42	9.02	52.23	61.25
293	11.82	9.19	52.87	62.07
303	12.02	9.29	53.11	62.40
400	13.64	10.15	55.88	66.03
500	14.90	10.98	58.23	69.22
600	15.88	11.72	60.30	72.02
700	16.62	12.36	62.15	74.51
800	17.19	12.93	63.83	76.76
900	17.64	13.43	65.39	78.82
1000	17.98	13.87	66.83	80.70

TABLE V

Heat capacity, heat content, free energy and entropy for nitryl chloride

Temp (K)	C_p^0	$(H_0—E_0^0)/T$	$-(F_0—E_0^0)/T$	S^0
100	8.44	8.04	45.88	53.91
200	10.74	8.80	51.65	60.45
273	12.26	9.53	54.50	64.03
293	12.62	9.73	55.17	65.09
303	12.84	9.85	55.44	65.29
400	14.25	10.73	58.35	69.08
500	15.41	11.56	60.84	72.40
600	16.29	12.27	63.01	75.28
700	16.97	12.91	64.96	77.87
800	17.48	13.44	66.71	80.15
900	17.88	13.91	68.31	82.22
1000	18.20	14.33	69.80	84.13

IV. REFERENCES

Decius, J. C., 1948, *J. Chem. Phys.* **16**, 1025.

Hariharan, T. A. 1958, *Proc. Ind. Acad. Sci.* **48**, 49.

Rolfe, Dodd and Woodward, L. A. 1956, *Trans. Farad. Soc.* **52**, 145.

Ryason, Raymond and Wilson, Kent, 1954, *J. Chem. Phys.* **22**, 2000.

21

A STUDY OF DEVELOPMENT DEFECTS AND TRACK STRUCTURES IN NUCLEAR EMULSIONS USING AMIDOL DEVELOPERS

O. N. KAUL

Saha Institute of Nuclear Physics, Calcutta.

(*Received, December* 30, 1960)

ABSTRACT. Development defects in nuclear emulsions, and also the dependence of track and grain structures on the various development parameters have been investigated.

Modified formulae have been suggested for the removal of microscopic fog, coloration defects, and also for the background eradication.

The procedures of investigation followed during the course of this work, differ from the ones adopted by others like Fatzer, Yagoda, Barschall, and Liebermann ; and the results, although identical in most of the cases, differ slightly in certain respects as reported.

Some work has been reported on the elimination of development defects by various workers, e.g., Yagoda, (1948), Liebermann and Barschall (1943) and others. The present aim of the author has been to make a comprehensive study of all development defects introduced by Amidol developers to compare the methods suggested by various workers for their elimination and also to suggest modified formulae suitable for work in this laboratory.

Besides this, a critical study of the track and grain structures pertaining to their dependence on various development parameters (temperature, time, and sodium sulphite concentration) has been made by methods somewhat different (from those adopted by Fatzer (1959).

Ilford C_2 nuclear emulsions of 100, 200 and 400 micron thickness were used and the problem studied under the following heads :

(1) Elimination of the development defects introduced by Amidol developers.

(2) Dependence of track and grain structures on the hot stage temperature,, hot stage time and sodium sulphite concentration.

(3) Removal of microscopic fog from the plates.

(4) Background eradication in nuclear emulsion by the accelerated fading of the latent images.

(1) *Elimination of the development defects introduced by the use of Amidol developers* :

Decrease in the development temperature gives rise to development defects, which are evidenced by a total or partial destruction of the developed image and also a coloration, extending to a considerable depth in the emulsion.

By a series of trials carried out by the author, it was found necessary to increase the ratio sodium sulphite/Amidol for the development temperatures from 18°C to 24°C.

It is an accepted fact that a decrease in the development temperature minimizes distortion in nuclear emulsions. Monothermal development suggested by Yagoda (1955) and Marguin (1957) in which temperature variations are replaced by P. H. variations, was avoided because of its complexity of operation. To avoid distortion, the development was, therefore, carried out at lower than usual temperatures which in turn gave rise to coloration defect, besides an irregularity in development.

To obviate this difficulty, four types of developers as indicated below were tried by the author.

TABLE I

Developer compositions : (in gms/lit. of the solution)

gms/lit. potassium bromide (KBr)	1.2	1.2	1.2	1.2
gms/lit. sodium sulphite (Na_2SO_3)	11	10	17	20
gms/lit. Amidol	4.0	2.8	2.8	2.8
gms/lit. boric acid (H_3BO_3)	30	20	20	20
Ratio of sodium sulphite : Amidol	2.75	3.57	6.07	7.14

By a comparative study of these formulae it was found that to develop reliably at low temperatures, it was necessary to increase the ratio sodium sulphite/Amidol to minimize the coloration. In certain cases of low sodium sulphite concentration, it was observed that the emulsion showed zones of good development, whereas the rest of the plate became useless. Further, in such cases the images were found to show a blue or red transparency. The development was carried out at temperatures higher and lower than 18°C and the coloration was found to be more predominant at lower temperatures, as well as to be a function of development time.

Results, almost resembling those indicated above, were reported by Birge (1954) and others. In some cases the images were completely destroyed,

but one thing is clear that this image destruction has nothing to do with the corrosion which sets in during prolonged fixation, and is more or less a surface phenomenon. In the present case, the disappearance of the image begins deep down in the emulsion.

These phenomena as already reported by James and Vonselow (1953) are due to the displacement of the adsorption equilibria of organic compounds and sodium sulphite, on silver halide grains. The following equation as suggested by Chateau (1956) can explain the phenomenon

$$2Ag\ NaSO_3 \rightarrow 2Ag + Na_2S_2O_6$$

$$AgS_2O_3^- + Ag^+ + H_2O \rightarrow Ag_2S + H_2SO_4$$

All the three sets of plates of 100, 200 and 400 micron thickness were tried, and it was found that all the three sets showed the coloration defect; but the thicker ones are less coloured than their thinner counterparts.

In conclusion, it was found necessary to choose a sodium sulphite to Amidol ratio which is 75% greater than the ratio adopted in Brussels or Chicago developers. Further, the following processing conditions used by the author were found to give best results :

TABLE II

Emulsion thickness (microns)	Water pre-soak		Developer pre-soak		Development time	Stop bath 1% CH_3COOH	
	Temp. T°C	Time Hrs.	Temp. T°C	Time Hrs.		Temp. T°C	Time Hrs.
100	4	0.4	4	0.4	Variable	4°C	0.4
200	4	1.0	4	1.0	Variable	4°C	1.0
400	4	2.6	4	2.6	Variable	4°C	2.6

(Microns)	Fixation (40% hypo)		Washing		Glycerinization One percent	
	Temp. T°C	Time Hrs.	Temp. T°C	Time Hrs.	Temp. T°C	Time Hrs.
100	18	3.5	8	4.0	6	0.5
200	18	8.0	8	10.0	6	1.0
400	18	24.0	8	28.0	6	2.0

Fog was removed by rubbing immediately after the stop bath treatment.

2) *Dependence of track and grain structures on the hot stage temperature, hot stage time and sodium sulphite concentration* :

In this connection various parameters, viz., diameter of the track grains, volumetric grain density, total gap length, mean gap length and blob density

were studied by the author, in the case of Ilford C_2 200 micron plates, some work has already been reported by Fatzer (1959) in this connection. Sodium sulphite/Amidol ratios and temperatures different from those used by Fatzer have been used. Results, although identical with those reported by Fatzer, differ in the peak values of the curves as reported :

a) Diameter of the track grains :

Mean grain diameters were plotted against the development time, for two temperatures and two sodium sulphite concentrations. The results obtained are plotted in Figs. 1 and 2.

Mean diameter of the track grains was found to increase rapidly with the time, in the region of under-development. It, however, attained a constancy in value for longer development periods (Figs. 1 and 2).

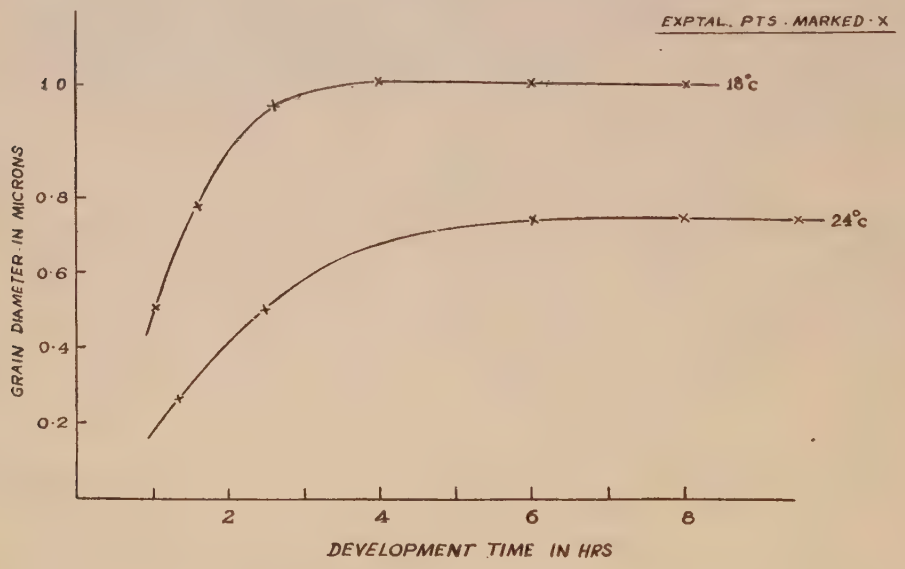

Fig. 1. Grain diameters plotted against development time for two different temperatures.

$$(\phi)\frac{\text{Sod. sulphite}}{\text{Amidol}} = 10$$

Further, it was obsered that an increase in the sodium sulphite concentration and development temperatures causes a decrease in the grain diameters.

b) Volumetric grain density :

Volumetric grain density was found to increase with an increase in the hot stage time and the sodium sulphite concentration. The observations are plotted in Fig. 3.

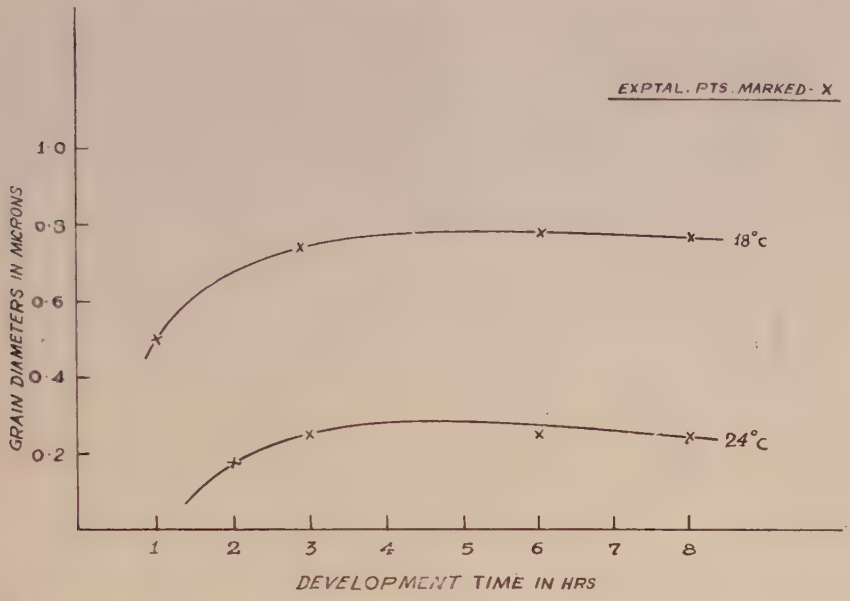

Fig. 2. Grain diameters plotted against the development time at two different temperatures.

$(\phi)\frac{\text{Sod. sulphite}}{\text{Amidol}} = 15$

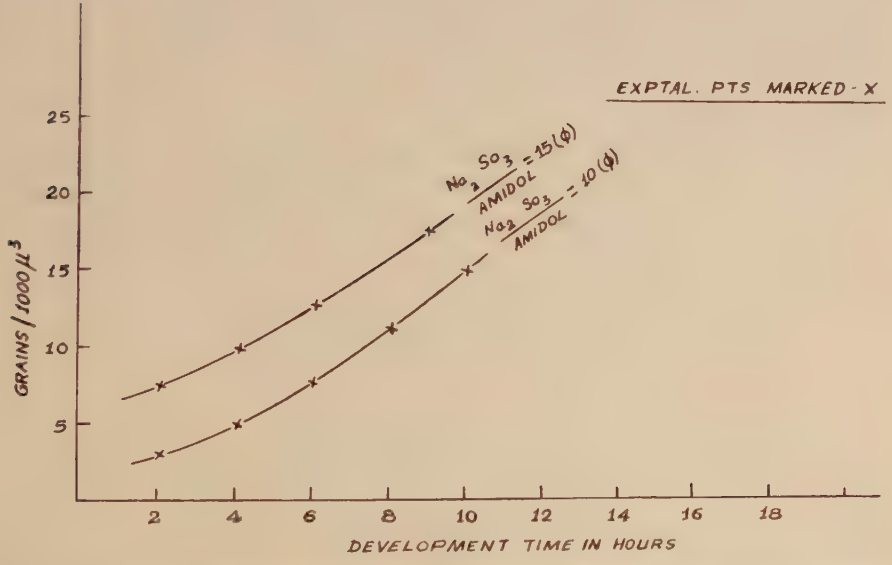

Fig. 3. Volumetric grain density plotted against hot stage time at two Na_2SO_3 concentrations.

1) *Total gap length* :

In the region of under-development total gap length was found to decrease with an increase in the development time. At longer development periods, the total gap length becomes constant. At normal developments, however, the total gap length decreases with increasing temperature and is independent of sodium sulphite concentration. (Fig. 4).

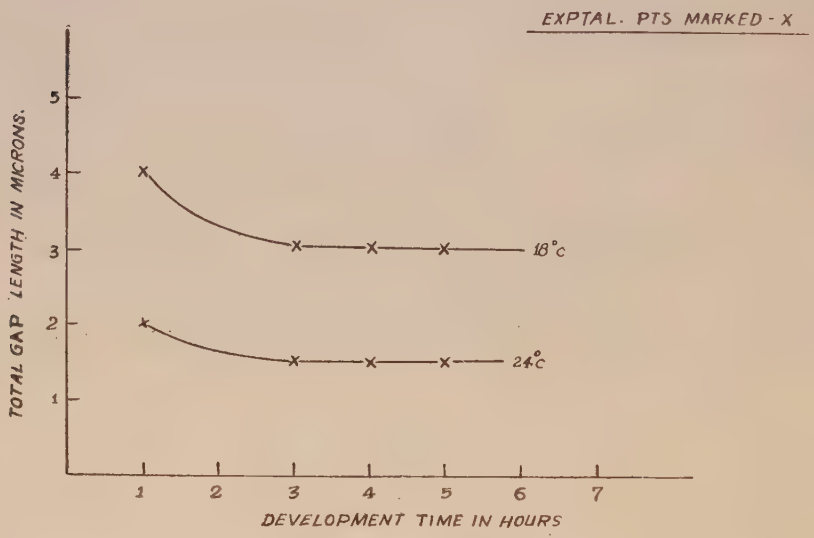

Fig. 4. Total gap length plotted against development time in hours.

2) *Mean gap length* :

The following points were observed in connection with the mean gap length, which was calculated by dividing the total gap length by the number of blobs.

1) M.G.L. is independent of the duration of hot stage time, excepting in the case of under-development.

2) M.G.L. decrease with an increase in temperature.

3) It does not vary with a change in sodium sulphite concentration.

5) *Variation of blob density.*

Blob density was calculated by dividing the number of blobs by the total length of the tracks. It was observed that the blob density increases in the region of under-development. Rise in temperature was found to cause a considerable rise in the blob density and after a certain value of development time, the blob density attained constancy in value. These observations are incorporated in Fig. 6.

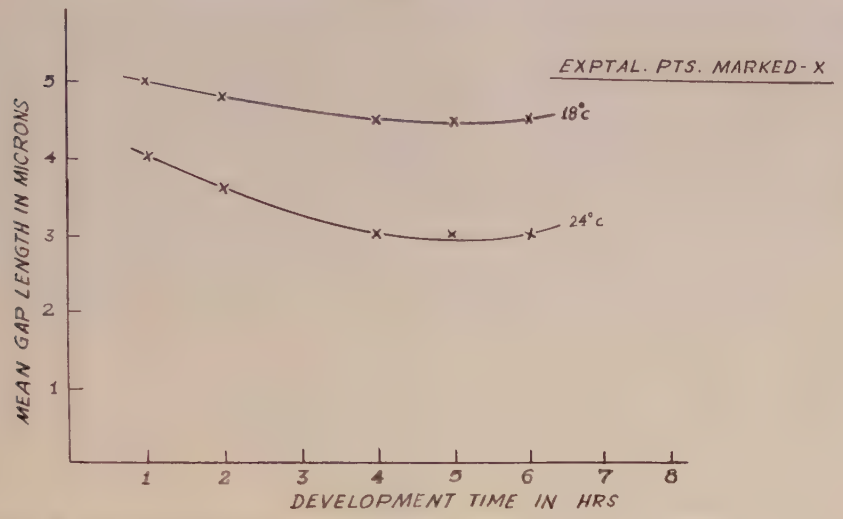

Fig. 5. Mean gap length plotted against the development time at two different temperatures.

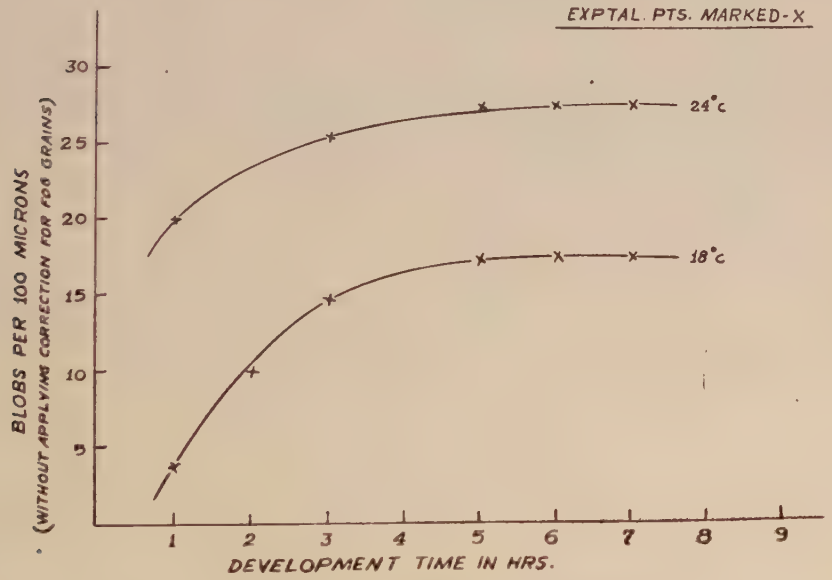

Fig. 6. Blob density plotted against development time in hrs.

(3) *Removal of microscopic fog from the plates* :

Background of developable but unexposed grains of silver bromide, manifesting itself in the form of microscopic fog, is a great handicap in the emulsion work. The idea underlying removal of fog is to develop an unexposed plate to reduce all the developable silver bromide grains, to free silver, which is then removed by reduction. Photographic reducers consist of oxidising agents which

oxidise free silver to a suitable salt, which in turn causes a reduction in the opacity of the image.

Well known formulae using potassium permanganate and potassium bichromate were used in this laboratory. Potassium permanganate formula was found to give better results, and also it was observed that potassium bichromate formula does not cause complete reduction and the grains thus reduced partially are again developable.

Out of the formulae suggested by various workers, the following formula modified by the author was found to give best results, without affecting silver bromide in the emulsion.

Sol. 1—Potassium permanganate— 3 gms water to make
1000 cc
Sol. 2—Sulphuric acid— 8 cc water to make
1000 cc.

Procedure :

The plate was first developed in the Eastman developer *D*–11 for a time greater than the usual, so as to be sure about the development of undesirable grains. The plate was then washed and immersed for about 40 minutes in a freshly prepared mixture of equal volumes of solutions 1 and 2. This procedure was tried for plates of various thicknesses. Following timings were found necessary:

Plate thickness (microns)	100	200	400
Time in minutes	30	40	55

Thus longer time was needed for the clearance of thick plates, as compared to their thinner counterparts. In order to remove the brown stain produced by potastium. permanganate, the plate was again washed and placed for 15 minutes in a 10% solution of sodium bisulphite. This procedure was found best for the removal of the background fog.

4) *Background eradication in nuclear emulsion*

The background is partly due to the accumulated latent images of α tracks and stars produced by traces of Ra and Th, normally present as impurities in the emulsion and partly due to the cosmic ray background.

It was found that storage for several hours in humid atmosphere goes a long way in accelerating the fading of latent images due to the background. The emulsions thus treated were then dessicated for 1 to 2 hrs. over calcium chloride.

Further, the effect of both the temperature and humidity on fading was investigated so as to find out their effect on the eradication of the background tracks.

Effect of temperature on fading :

The variation of the fading rate with the storage temperature may be determined from a consideration of the effect of temperature on the velocity of a gas solid chemical reaction, such as is assumed to occur during fading between certain constituents of the atmosphere and the silver development centres of the exposed emulsion. This gives a form of the Arrhenius relation with $-dN/dt$, the rate of disappearance of the development centres, as the equation

$$-\frac{dN}{dt} = Ce^{-K/T}$$

where C and K are constants and T the absolute storage temperature. The equation shows that the fading produced under otherwise fixed conditions will be an exponential function of the reciprocal of the absolute temperature, a result confirmed by Farragi (1949). This shows the effect of storage temperature on the background eradication and it is found that the experimental findings are in accord with the theory.

Effect of humidity on fading:

According to Albouy and Farragi (1949) fading is a result of the oxidation of the development specks by the atmospheric oxygen in the presence of water, the reaction as proposed by Albouy and Farragi proceeds as

$$Ag+O+H_2O \rightarrow Ag+2OH^-$$

It is evident that the presence of an excess of OH^- ions i.e. PH value above 7, will act to inhibit the reaction, while the more acid conditions accelerate it. Thus, an increase in the humidity causes a decrease in the fading rate.

The following graph showing the effect of both temperature and humidity on the background eradication is in accord with the theory.

Theoretical investigations due to Beiser (1951) also lead to the following equation for the fading coefficient

$$\frac{D_0-D}{D_0} = 1-\text{Exp.}(-Ct)$$

where D_0 = grain density produced upon immediate development

D = grain density after a time t

C = constant depending upon the size of Ag specks

The fading coefficient plotted as a function of t, for various values of C, is in agreement with the experimental curves.

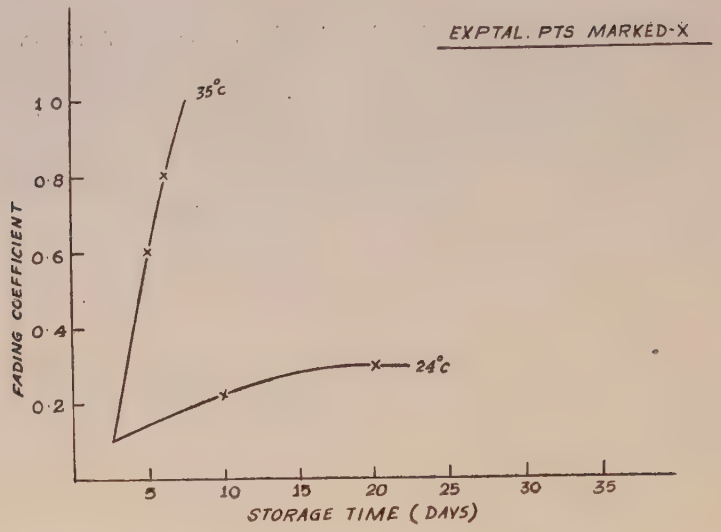

Fig. 7. The variation of the fading coefficient with the time of storage at various temperatures.

ACKNOWLEDGMENTS

The author expresses his deep sense of gratitude to Prof. B. D. Nag Chaudhuri, under whose direction and guidance this work has been carried out. The author is also thankful to Mr. S. K. Mukherjee for providing the laboratory facilities ; and to Messrs. Naresh Sen and Barin Chatterjee for their valuable assistance.

REFERENCES

Albouy, G. and Farragi, H., 1949, *J. Phys. Et. Radium.*
Beiser, A., 1951 *Phys. Rev.*, **81**, 153.
Birge, 1954, *Bull. Uni. Cal. Rad. Lab.*, September 8, 2690.
Chateau, H., 1956, *Sci. Ind. Phot.*, **27**, 81.
Fatzer, G- D., 1959, *Rev. Sci. Inst.*, **30**, 22.
James, H. and Vogu, 1952, *Sci. Ind. Phot.*, **23**, 144.
James T. H. and Vanselow, Collig., *Revue Optique Paris*, 122, Emul. Phot.
Liebermann, L. N. and Barschall, H. H., 1943, *Rev. Sci. Inst.*, **14**, No. 4.
Marguin, G., 1957, *Sci. Ind. Phot.*, **28**, 321.
Yagoda, H., 1948, *Phys. Rev.*, **73**, 634.
Yagoda, H., 1955, *Rev. Sci. Inst.*, **26**, 263.

22

INTERPENETRATION OF TWO IONIZED GAS CLOUDS

J. N. TANDON*

Department of Physics, University of Delhi, Delhi-8

(*Received, October* 26, 1960)

ABSTRACT. Collisions of two ionized gas clouds have been considered and it is shown that the counter streaming will, in general, be unstable and the double stream will form small clouds of space charge at the expense of streaming energy of the clouds. These small clouds are responsible for the geomagnetic storms and for the generation of radio noise from colliding galaxies.

INTRODUCTION

Collision of two fully ionized gas clouds is of considerable importance in explaining the geomagnetic storms and the generation of radio noise from the colliding galaxies. It is found that the counter streaming of gas cloud will in general be unstable except for the case when the density of one of the streams is extremely low as compared to that of the other. The double stream will form small clouds of space charge at the expense of the streaming energy of the clouds. These small clouds may be able to reach the earth and diffuse through the geomagnetic field producing geomagnetic storm. These space charge clouds, because of their stray electric fields, may be responsible for the generation of radio noise from the colliding galaxies.

COUNTERSTREAMING OF IONIZED GAS CLOUDS

Suppose that a completely ionized neutral gas cloud of initial uniform density N_{o1} electrons and N_{o1} protons per cm^3 moving with initial uniform velocity $\mathbf{V}_{o1}$. Let a similar stream with density N_{o2} electrons and N_{o2} protons per cm^3 be moving with velocity $-\mathbf{V}_{o2}$. We shall further assume that the temperature and velocity of each stream be such that the thermal motion among the particles and the collisions by coulomb interaction may be ignored.

Let us consider that these two gas clouds impinge upon one another. After the counterstreaming we shall assume the deviation in the densities and velocities from the initial uniform streaming to be of the first order only and are regarded as functions of position and time. We shall use the subscripts 1 and 2 to refer to the two streams and subscripts e and p to denote the electrons and protons respectively. Thus we let their densities and velocities be

* Senior Fellow of University Grants Commission, India.

$$N_{e1} = N_{o1} + n_{e1}; \qquad N_{p1} = N_{o1} + n_{p1} \qquad \ldots (1)$$

$$N_{e2} = N_{o2} + n_{e2}; \qquad N_{p2} = N_{o2} + n_{p2} \qquad \ldots (2)$$

$$\mathbf{V}_{e1} = \mathbf{V}_{o1} + \mathbf{v}_{e1}; \qquad \mathbf{V}_{p1} = \mathbf{V}_{o1} + \mathbf{v}_{p1} \qquad \ldots (3)$$

$$\mathbf{V}_{e2} = -\mathbf{V}_{o2} + \mathbf{v}_{e2}; \qquad \mathbf{V}_{p2} = -\mathbf{V}_{o2} + \mathbf{v}_{p2} \qquad \ldots (4)$$

Then if the electric field is E, we have the Poisson equation

$$\text{div } E = 4\pi e(n_{e1} - n_{p1} + n_{e2} - n_{p2}) \qquad \ldots (5)$$

The equations of motion are

$$\left[\frac{\partial}{\partial t} + (\mathbf{V}_{e1} \cdot \text{grad})\right] \mathbf{V}_{e1} = \frac{e}{m}\mathbf{E} \qquad \ldots (6)$$

$$\left[\frac{\partial}{\partial t} + (\mathbf{V}_{p1} \cdot \text{grad})\right] \mathbf{V}_{p1} = -\frac{e}{M}\mathbf{E} \qquad \ldots (7)$$

$$\left[\frac{\partial}{\partial t} + (\mathbf{V}_{e2} \cdot \text{grad})\right] \mathbf{V}_{e2} = \frac{e}{m}\mathbf{E} \qquad \ldots (8)$$

$$\left[\frac{\partial}{\partial t} + (\mathbf{V}_{p2} \cdot \text{grad})\right] \mathbf{V}_{p2} = -\frac{e}{M}\mathbf{E} \qquad \ldots (9)$$

and the equations of continuity are

$$\left[\frac{\partial}{\partial t} + (\mathbf{V}_{e1} \cdot \text{grad})\right] N_{e1} + N_{e1} \text{ div } \mathbf{V}_{e1} = 0 \qquad \ldots (10)$$

$$\left[\frac{\partial}{\partial t} + (\mathbf{V}_{p1} \cdot \text{grad})\right] N_{p1} + N_{p1} \text{ div } \mathbf{V}_{p1} = 0 \qquad \ldots (11)$$

$$\left[\frac{\partial}{\partial t} + (\mathbf{V}_{e2} \cdot \text{grad})\right] N_{e2} + N_{e2} \text{ div } \mathbf{V}_{e2} = 0 \qquad \ldots (12)$$

$$\left[\frac{\partial}{\partial t} + (\mathbf{V}_{p2} \cdot \text{grad})\right] N_{p2} + N_{p2} \text{ div } {}_{p}\mathbf{V}_{2} = 0 \qquad \ldots (13)$$

Here e and m are the electronic charge and mass respectively and $-e$ and M are the respective quantities for the protons. Combining equations of the motion (Eqns. (6) to (9)) and equations of continuity (Eqns. (10) to (12)) and using Eqns (1) to (5) we get after some simplification

$$\left[\frac{\partial}{\partial t} + (\mathbf{V}_{o1} \cdot \text{grad})\right]^2 n_{e1} = -\omega^2{}_{e1}(n_{e1} - n_{p1} + n_{e2} - n_{p2}) \qquad \ldots (14)$$

$$\left[\frac{\partial}{\partial t} + (\mathbf{V}_{o1} \cdot \text{grad})\right]^2 n_{p1} = \omega^2{}_{p1}(n_{e1} - n_{p1} + n_{e2} - n_{p2}) \qquad \ldots (15)$$

$$\left[\frac{\partial}{\partial t}-(\mathbf{V}_{o2}.\ \text{grad})\right]^2 n_{e2} = -\omega^2_{e2}(n_{e1}-n_{p1}+n_{e2}-n_{p2}) \quad \ldots \quad (16)$$

$$\left[\frac{\partial}{\partial t}-(\mathbf{V}_{o2}.\ \text{grad})\right]^2 n_{p2} = \omega^2_{p2}(n_{e1}-n_{p1}+n_{e2}-n_{p2}) \quad \ldots \quad (17)$$

Here ω's represent the electron or proton plasma frequencies in the two streams, viz,

$$\omega_e^2 = \frac{4\pi N_o e^2}{m} \qquad \text{and} \qquad \omega_p^2 = \frac{4\pi N_o e^2}{M} \quad \ldots \quad (18)$$

Substracting Eq. (15) from equation (14) and Eq. (17) from Eq. (16) and putting

$$a_1 = n_{e1}-n_{p1} \qquad \text{and} \qquad a_2 = n_{e2}-n_{p2} \quad \ldots \quad (19)$$

$$\omega_1^2 = \omega_{e1}^2+\omega_{p1}^2 \qquad \text{and} \qquad \omega_2^2 = \omega_{e2}^2+\omega_{p2}^2 \quad \ldots \quad (20)$$

We find

$$\left[\frac{\partial}{\partial t}+(\mathbf{V}_{o1}\ .\ \text{grad})\right]^2 a_1 = -\omega_1^2(a_1+a_2) \quad \ldots \quad (21)$$

$$\left[\frac{\partial}{\partial t}-(\mathbf{V}_{o2}.\ \text{grad})\right]^2 a_2 = -\omega_2^2(a_1+a_2) \quad \ldots \quad (22)$$

The solutions involving a's can be represented as

$$a = a_o \exp i(\sigma t+\vec{\kappa}\ .\ \mathbf{r}) \quad \ldots \quad (23)$$

here $\boldsymbol{r}$ is the space vector.

In the solution of the above type, with a given real $\vec{\kappa}$, the counterstreaming will be unstable for which σ is a complex quantity. In this case the amplitude of the corresponding oscillations can grow indifinitely. The minimum value of wave number κ_{min} for which this is possible gives the maximum value of the wave length λ_{max} at which there is instability. The double stream will then be unstable for complex value of σ and will form small clouds of space charge with maximum length λ_{max} at the expense of the streaming energy of the beam.

To determine the dispersion relation between σ and κ we substitute equation (23) into Eqns. (21) and (22) and after rearrangement we get

$$[\{\sigma+(\mathbf{V}_{o1}\ .\ \vec{\kappa})\}-\omega_1^2]a_{o1} = \omega_1^2 a_{o2} \quad \ldots \quad (24)$$

and

$$[\{\sigma-(\mathbf{V}_{o2}\ .\ \vec{\kappa})\}-\omega_2^2]a_{o2} = \omega_2^2 a_{o1} \quad \ldots \quad (25)$$

Elimination of a_{o1} and a_{o2} from Eqns. (24) and (25) gives the relations between σ and κ, viz..

$$\{\sigma+(\mathbf{V}_{o1}\cdot\vec{\kappa})\}^2\{\sigma-(\mathbf{V}_{o2}\cdot\vec{\kappa})\}^2-\omega_1^2\{\sigma-(\mathbf{V}_{o2}\cdot\vec{\kappa})\}^2$$
$$-\omega_2^2\{\sigma+(\mathbf{V}_{o1}\cdot\vec{\kappa})\}^2=0 \qquad \ldots (26)$$

DISPERSION RELATIONS

To study the nature of σ for all real values of κ we substitute

$$\left.\begin{aligned}\mathbf{V}_{o1}+\mathbf{V}_{o2}&=2U\\ \mathbf{V}_{o1}-\mathbf{V}_{o2}&=2V\end{aligned}\right\} \qquad \ldots (27)$$

$$p=\omega+\mathbf{V}\cdot\vec{\kappa} \qquad \ldots (28)$$

and

$$\Omega=\mathbf{U}\cdot\vec{\kappa} \qquad \ldots (29)$$

in dispersion relation (26) and obtain

$$\{p^2-\Omega^2\}^2-(\omega_1^2+\omega_2^2)(p^2+\Omega^2)+2(\omega_1^2-\omega_2^2)p\Omega=0 \qquad \ldots (30)$$

Further, let us put

$$N_{o2}=bN_{o1} \qquad \ldots (31)$$

Thus we have

$$\omega_2^2=b\omega_1^2$$
$$=b\omega^2 \text{ (say)} \qquad \ldots (32)$$

and Eq. (30) reduces to

$$(p^2-\Omega^2)^2-(1+b)\omega^2(p^2+\Omega^2)+2(1-b)\omega^2p\Omega=0 \qquad \ldots (33)$$

This is the most general relation and difficult to solve exactly. We shall therefore study Eq. (33) for some specific cases of astrophysical interest.

Case (i) $b\simeq 1$. Let us first consider that the streams have initially the same densities. Thus for $b=1$ and Eq. (33) reduces to

$$(p^2-\Omega^2)^2-2\omega^2(p^2+\Omega^2)=0$$

or

$$p^4-2p^2(\Omega^2+\omega^2)+\Omega^2(\Omega^2-2\omega^2)=0 \qquad \ldots (34)$$

It can readily be shown that for all real values of $\vec{\kappa}$ and for

$$\Omega^2>2\omega^2 \qquad \ldots (35)$$

p^2 is always real and positive. However, there exists a real and negative value for p^2 provided

$$\Omega^2 < 2\omega^2 \qquad \ldots \quad (36)$$

Let this value of p^2 be $-q^2$. Thus we have

$$\sigma = -\mathbf{V}.\vec{\kappa} + iq \qquad \ldots \quad (37)$$

and hence for such a value of σ it is evident that the oscillations will go on build-ing up with the time and will therefore make the whole system unstable. The minimum value of $\vec{\kappa}.\vec{\kappa}$, κ_{min} for such system may be evaluated from

$$\vec{\kappa}_{min}.\boldsymbol{U} = \sqrt{\frac{8\pi N_o e^2(m+M)}{mM}} \qquad \ldots \quad (38)$$

and

$$\lambda_{max} = \frac{2\pi}{\kappa_{min}} \qquad \ldots \quad (39)$$

Kahn (1957) has discussed a particular case in which the two streams of equal density are moving in opposite direction having equal velocity U along the x-axis. For this case we obtain

$$\lambda_{max} = \sqrt{\frac{\pi mM}{2N_o e^2(m+M)}} \qquad \ldots \quad (40)$$

Our results are somewhat different from those of Kahn (1957) because of his assuming only the electrons interactions. The protons were assumed to provide a uniform background of positive charge because of their heavier mass, which in our opinion may not be a valid assumption.

Let us further assume that one of the streams is stationary, say $\mathbf{V}_{o2} = 0$. This gives

$$\mathbf{U} = \mathbf{V} \qquad (41)$$

and hence the stream will again be unstable and the maximum stable length will be given by equation (39) in conjunction with equation (38).

Case (ii) $b \approx 0$. Let us assume that a gas cloud is impinging into vacuum. Thus for $b \approx 0$ we get from Eq. (33) after simplification

$$(p^2 - \Omega^2)^2 - \omega^2(p - \Omega)^2 = 0 \qquad \ldots \quad (42)$$

It is evident from Eq. (42) that p and hence σ is always real for all real values of κ. Therefore the stream will plunge into vacuum without having any instability.

When $b>>|$ the situation is similar to that discussed for case (ii). For $0 \leqslant b \leqslant |$ the problem cannot be solved explicitly. The above discussion and the inspection of Eq. (33) reveals that the beam will in general be unstable except for $b \approx 0$ and for $b>>|$

DISCUSSION OF RESULTS

It has been shown above that two penetrating streams will, in general, be unstable even when one of the streams is at rest. This is of great significance in regard to the magnetic storm theory, where the solar ion streams emanating from the disturbed solar regions produce geomagnetic storms on reaching the earth. These solar-ion streams while penetrating the solar atmosphere will become unstable and will form small clouds of space charge moving towards the earth. These clouds on entering the geomagnetic field may diffuse into the earth's magnetic field and a belt of trapped particles may be produced within the geomagnetic field, which may be responsible for the main phase of the geomagnetic storm. Kahn (1957) has alternatively suggested that the counter-streaming will be stopped because of this instability. Such an effect would prevent the passage of solar-ion stream through the solar atmosphere and inter-planetary matter. Thus, in our opinion, such an interpretation of instability may not be probable.

This instability and the formation of small clouds of space charge may also explain the generation of radio noise from the colliding galaxies e.g. Cygnus A, NGC 5128 and NGC 1275. These space charge clouds will produce the stray electric fields and the charged particles moving under the influence of this field may be responsible for the radio emission.

REFERENCE

Kahn, F. D., 1957, *J. Fluid Mech.*, **2**, 601.

23

GROWTH OF HYDROMAGNETIC SHOCK WAVES

I. J. SINGH

Oil and Natural Gas Commission, Dehradun, India

AND

K. P. CHOPRA

Engineering Center, University of Southern California

Los Angeles, California, U.S.A.*

(*Received, September* 21, 1960)

ABSTRACT. In this technical note we consider the influence of a transverse magnetic field on the formation of a shocks wave in an electrically conducting field. We conclude that the presence of a transverse magnetic field is conducive to the growth of compression waves and tho decay of the expansion waves.

It is well known that the ordinary hydrodynamic compression shock wave involves an increase in entropy and that the rarefaction shock wave decays immediately into a continuous expansion wave. This is so because in a compression wave, the waves nearer the source tend to overtake those further from it with the result that the wave profile becomes more and more steep until the pressure gradients become infinite. In this way a compression shock is formed which grows in strength as the process continues. In a rarefaction shock, on the other hand, the waves nearer the shock lag more and more behind those in front of it, the wave profile flattens till the pressure gradients vanish and ultimately no dis continuity effects are observed. In fact if a rarefaction shock is established, even momentarily, it would decay immediately into a continuous expansion wave. We will consider, in this note, the influence of a transverse magnetic field on the formation of a shock wave in an electrically conducting fluid. It will be seen that the presence of a transverse magnetic field is conducive to the formation of a shock wave.

For the sake of simplicity we will consider a plane one-dimensional shock wave propagating in a fluid of infinite electrical conductivity and specific volume τ with an external magnetic field H oriented in a direction normal to the direction in which the shock propagates. We define the quantities $p^{\times}$ and $c^{\times}$ according to Hoffmann *et al.*, 1950.

$$p^{\times} = p + \frac{H^2}{8\pi}, \quad \text{and} \quad c^{\times} = (c^2 + v^2_{ALF})^{\frac{1}{2}} \qquad \ldots (1)$$

*Present Address: Aerodynamics Laboratory, Polytechnic Institute of Brooklyn Freeport, N. Y., U. S. A.

These quantities take account of the contributions of the hydromagnetic interaction to the pressure p and the velocity of sound c through the magnetic pressure $(H^2/8\pi)$ and the Alfven speed $v_{ALF} = H(\tau/4\pi)^{\frac{1}{2}}$. We will call $p^\times$ and $c^\times$ the total pressure and the modified velocity of sound respectively.

Let us now suppose that the properties of the fluid at two adjacent points differ in magnitude by $d\tau$, dH, dv, $dp^\times$ and $dc^\times$ where v denotes the gas speed. We also assume that the respective parts of the wave passing through these points differ in speed of propagation by dv_ω. For the sake of simplicity, let us further assume that the gradients of temperature and velocity are small so that the dissipative effects of viscosity and heat conduction are negligible. Therefore each elementary part of the wave travels with the local speed of sound with respect to the fluid. The velocity of propagation v_ω of this part of the wave with reference to a fixed coordinate system is

$$V_\omega = v + c^\times \qquad \ldots \quad (2)$$

and the velocity of propagation of an adjacent part of the wave is

$$v_\omega + dv_\omega = v + dv + c^\times + dc^\times \qquad \ldots \quad (3)$$

so that

$$\frac{dV_\omega}{dp^\times} = \frac{dv}{dp^\times} + \frac{dc^\times}{dp^\times} \qquad \ldots \quad (4)$$

Let us assume that the entire fluid was initally at rest with uniform pressure and temperature, and that each particle of the fluid undergoes isentropic changes. Therefore, the increments in pressure and density between adjacent particles obey the relation

$$c^{\times 2} = -\tau^2 \frac{dp^\times}{d\tau} \qquad \ldots \quad (5)$$

which yields on differentiation

$$2c^\times \frac{dc^\times}{dp} = -\frac{d\tau}{dp^\times} \frac{d}{d\tau} \left(\tau^2 \frac{dp^\times}{d\tau} \right) \qquad \ldots \quad (6)$$

Again it can be shown from the equations of constant mass flux and constant momentum flux that

$$\frac{dv}{dp^\times} = \frac{\tau}{c^\times} \qquad \ldots \quad (7)$$

On carrying out the substitutions from (6) and (7) in (4) we finally obtain

$$\frac{dV_\omega}{dp^\times} = -\frac{\tau}{2c^\times}\frac{(d^2p^\times/d\tau^2)}{(dp^\times/d\tau)} \qquad \ldots \quad (8)$$

Now if $(dV_\omega/dp^\times)$ is positive, the high pressure parts of the wave overtake the low pressure parts and a wave of compression steepens as it progresses. Similarly a wave of rarefaction becomes less steep. On the other hand if $(dV_\omega/dp^\times)$ is negative, a wave of compression becomes less steep and a wave of rarefaction steepens into a compression shock.

A fluid is said to be thermodynamically stable if it does not collapse or expand catastrophically. For a fluid to be thermodynamically stable, $dV_\omega/dp^\times$ must be positive. It follows from (8) that the sign of $dV_\omega/dp^\times$ depends on the sign of

$$\frac{d^2p^\times}{d\tau^2} = \frac{d^2p}{d\tau^2} + \frac{3H^2}{4\pi\tau^2} \qquad \ldots \quad (9)$$

From the considerations outlined above, we immediately arrive at the following conclusions :

(i) Compression waves steepen and rarefaction waves flatten when

$$\tau^2\frac{d^2p}{d\tau^2} + \frac{3H^2}{4\pi} > 0 \qquad \ldots \quad (10)$$

This happens when

either (*a*) $d^2p/d\tau^2$ is positive

or (b) $d^2p/d\tau^2$ is negative, and

$$\left|\frac{d^2p}{d\tau^2}\right| < \frac{3H^2}{4\pi\tau^2}$$

Therefore, a flattening wave of compression will begin to steepen as soon as a magnetic field of suitable strength is switched on.

(ii) Compression waves flatten and rarefaction waves steepen when

$$\tau^2\frac{d^2p}{d\tau^2} + \frac{3H^2}{4\pi} < 0 \qquad \ldots \quad (11)$$

This happens when $(d^2p/d\tau^2)$ is essentially netgative and

$$\left| \frac{d^2p}{d\tau^2} \right| > \frac{3H^2}{4\pi\tau^2} \quad \ldots \quad (12)$$

Hence it may be concluded that the magnetic field enhances the steepening of a compression wave and flattening of a rarefaction wave. Hence the presence of a transverse magnetic field is conducive to the growth of compression waves and the decay of the expansion waves.

REFERENCES

Hoffmann, F. de and Teller, E., 1950. *Phys. Rev.*, **80**, 692.

24

ELECTRONIC SPECTRA OF *m*-CHLOROPHENOL AND *o*-BROMOANISOLE IN DIFFERENT STATES*

T. N. MISRA AND S. B. BANERJEE

Optics Department, Indian Association for the Cultivation of Science, Calcutta-32

(*Received, February* 25, 1961)

ABSTRACT. The ultraviolet absorption spectra of *m*-chlorophenol and *o*-bromoanisole in the vapour, liquid and solid states have been studied. In the vapour phase, *m*-chlorophenol yields about fifty sharp bands with the 0,0 band at 35761 cm^{-1}. The observed frequencies are 151, 190 and 235 cm^{-1} in the ground state and 120, 180, 225, 362, 503, 612, 737, 858, 959, 1029 and 1086 cm^{-1} in the excited state. In the spectrum of the liquid, the bands are broad and the 0,0 band is displaced by about 260 cm^{-1} towards red with respect to its position in the vapour phase. When the liquid is frozen and cooled to $-180°C$, no further change in the spectrum is observed.

In the spectrum of *o*-bromoanisole in the vapour state the 0,0 band is at 35615 cm^{-1} and the observed excited state frequencies are 221, 358, 517, 632, 685, 744, 955, 1031 and 1233 cm^{-1}. The bands observed in the spectrum of the liquid are broad and the 0,0 band is shifted by about 390 cm^{-1} towards longer wavelengths from its position in the spectrum of the vapour. With solidification of the liquid and cooling to $-180°C$, no appreciable change is observed in the spectrum.

INTRODUCTION

The ultraviolet absorption spectra of a large number of disubstituted benzene compounds in different states have been investigated in this laboratory to study the influence of intermolecular forces on the position and structure of absorption bands in the liquid and solid states. The present work is an extension of such investigations to the case of *m*-chlorophenol and *o*-bromoanisole.

It appeared that the ultraviolet absorption spectra of these compounds in any state had not been studied by any previous worker. The absorption spectra of the compounds in the vapour, liquid and solid states have, therefore, been analysed and the changes in the spectra observed with the change of state and temperature have been discussed in the present paper.

EXPERIMENTAL

The experimental set-up was the same as that described in an earlier paper (Banerjee, 1956). Chemically pure *m*-chlorophenol and *o*-bromoanisole obtained from Fisher Scientific Co., U.S.A., were used after fractional and

* Communicated by Professor S. C. Sirkar.

repeated vacuum distillation. For studying the absorption spectrum in the vapour state, cells of length 50 cm and 20 cm respectively and provided with quartz windows and a bulb attached to a side tube for containing the liquid, were used. In order to obtain suitable pressure of the absorbing vapour, the temperature of the liquid was varied from −20°C to 32°C by immersing the container in suitable low temperature baths while the absorption tube was kept at the room temperature (about 32°C).

Thin films of the substances of thickness of the order of a few microns were required to produce bands in the liquid and solid states. The spectrograms were taken on Agfa Isopan films with a Hilger E l spectrograph giving a dispersion of about 3A per mm. in the 2600Å region. Microphotometric records were taken with a Kipp and Zonen type Moll microphotometer and the absorption spectra were calibrated with the help of microphotometric records of iron arc spectrum photographed on each spectrogram as explained in a previous paper (Banerjee, 1956).

RESULTS AND DISCUSSION

The microphotometric records of the absorption spectra of *m*-chlorophenol and *o*-bromoanisole are reproduced in Figs. 1, 2, 3 and 4. The wave numbers of the bands with their approximate visual intensities and probable assignments are given in Tables I, II, III and IV.

The near ultraviolet absorption system in the case of the molecules of both the compounds, belonging to C_s point group, is due to an allowed $A'-A'$ transition, with the transition moment lying in the plane of the molecule. Accordingly, the spectrum in each case consists of a number of intense bands with a strong 0, 0 band. The results obtained for the two compounds are discussed separately in the following paragraphs.

m-Chlorophenol

About fifty sharp bands have been recorded in the spectrum due to *m*-chlorophenol in the vapour state. The most intense band at 35761 cm^{-1} on the long wavelength side of the spectrum which persists at low pressure of the absorbing vapour has been taken as the 0, 0 band. The other bands may then be explained in terms of frequencies 151, 190 snd 235 cm^{-1} in the ground state and 120, 180, 225, 362, 503, 569, 612, 737, 858, 959, 1029 and 1086 cm^{-1} in the excited state. The Raman spectrum of the substance was studied by Kohlrausch and Pongratz (1935) who reported the frequency shifts, 193(3), 241(2b), 409(3), 527(1), 684(3), 769(0), 890(1), 995(6), 1066(3), 1088($\frac{1}{2}$), 1157(0), 1253(2b), 1304(0), 1583(3b) and 3070(0) cm^{-1}, the intensities being given in the parentheses. It can be seen that the frequencies observed in the present investigation can be correlated with the

TABLE I

Ultraviolet absorption bands of *m*-chlorophenol in the vapour state

Wave No. (cm^{-1}) and Intensity	Assignment	Wave No. (cm^{-1}) and Intensity	Assignment
35526 (m)	0−235	36988 (vw)	0+1227
			0+2×612
35572 (w)	0−190		
		37071 (w)	0+959+362
35610 (w)	0−151		
		37212 (vw)	0+858+612
35678 (m)	0−83		0+959+503
35710 (m)	0−235+180	37232 (vw)	0+2×737
35761 (s)	0,0	37316 (w)	0+1555
			0+959+612
35793 (w)	0+180−151		0+1029+503
35834 (m)	0+225−151	37386 (m)	0+1625
35881 (s)	0+120	37470 (m)	0+2×858
			0+959+737
35941 (m)	0+180		
		37568 (m)	0+959+858
35986 (m)	0+225		
		37604 (m)	0+1086+737
36123 (w)	0+362		0+3×612
36264 (w)	0+503	37670 (s)	0+2×959
36330 (w)	0+569	37700 (vw)	0+1086+858
36373 (m)	0+612	37736 (vw)	0+959+1029
36498 (m)	0+737	37810 (vw)	0+959+1086
			0+2×1029
36619 (m)	0+858		
		37856 (w)	0+1029+1086
36653 (m)	0+858+180−151		
		37949 (m)	0+2×1086
36672 (w)	0+858+225−151		
	0+959−235+180	37982 (m)	0+3×737
36720 (s)	0+959	38033 (m)	0+2×959+362
36753 (w)	0+959+180−151	38346 (m)	0+3×858
36790 (m)	0+1029	38420 (s)	0+2×959+737
36847 (s)	0+1086	38526 (w)	0+2×959+858
		38643 (s)	0+3×959

TABLE II

Ultraviolet absorption spectra of *m*-chlorophenol in the liquid and solid states

Liquid at 32°C		Solid at −180°C	
Wave No. (cm^{-1}) and Intensity	Assignment	Wave No. (cm^{-1}) and Intensity	Assignment
35508 (sbb)	0,0	35564 (sb)	0,0
36447 (sbb)	0+939	36485 (sb)	0+921
37398 (wb)	0+2×939	37414 (wbb)	0+2×921

ground state frequencies observed by Kohlrausch and Pongratz. The upper state frequencies 180 and 225 cm^{-1} correspond probably to the Raman frequencies 193 and 241 cm^{-1}; the observed ground state frequencies 190 and 235 cm^{-1} are also in good agreement with the Raman data. The frequency 120 cm^{-1} may be

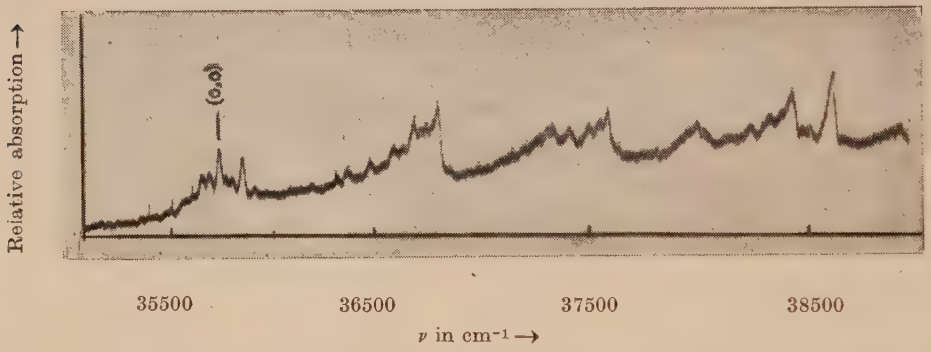

Fig. 1. Microphotometric record of the ultraviolet absorption spectrum of *m*-chlorophenol in the vapour state.

the excited state value of the observed ground state frequency 151 cm^{-1}. Though Kohlrausch *et al.* did not report any Raman shift of this magnitude, we are probably justified in taking 151 cm^{-1} as a fundamental frequency, because such low frequency fundamentals are usually observed in the ultraviolet absorption spectra of phenol compounds (Swamy, 1953; Ramasastry, 1951). This frequency probably represents an out of plane deformation vibration. The other excited state frequencies 362, 503, 612, 737, 858, 959 and 1029 cm^{-1} can be correlated with the ground state frequencies 409, 527, 684, 769, 890, 995 and 1066 cm^{-1} respectively, observed in Raman effect. The strong band at 36847 cm^{-1} may be analysed as 0+1086 cm^{-1}, there being two weak ground state frequencies 1088 and 1157 cm^{-1} reported by Kohlrausch *et al.* Similarly, the weak band at 36988 and 37316 cm^{-1} may be assigned as 0+1227 and 0+1555 cm^{-1} respectively,

since there are two Raman lines at 1253 and 1583 cm^{-1}, but these two bands can also be alternatively assigned as combination frequencies as shown in Table I. The band at 35710 cm^{-1}, on the longer wavelength side of the 0, 0 band at a distance of 51 cm^{-1} and those at 35793 and 35834 cm^{-1} with shifts of 32 and 73 cm^{-1} from the 0, 0 band on the short wavelength side may be explained as $v' \rightarrow v$ transitions as shown in Table I.

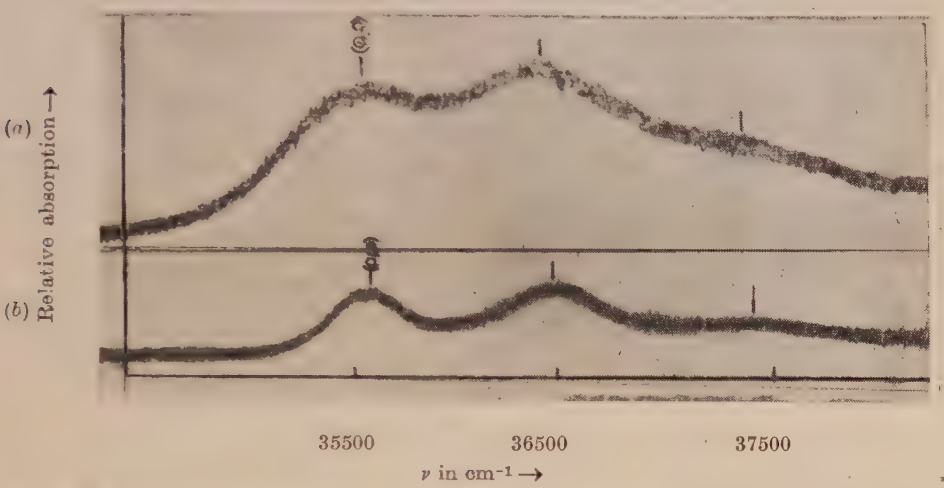

Fig. 2. Microphotometric records of the ultraviolet absorption spectra of *m*-chlorophenol. (*a*) Liquid at 32°C. (*b*) Solid at −180°C.

In the spectrum of the liquid there are three broad bands with centres approximately at 35508, 36447 and 37398 cm^{-1}, the centre of the first band being taken as the position of the 0, 0 band. Thus it is seen that the liquefaction of the vapour results in a shift of about 260 cm^{-1} towards red of the 0, 0 band. The three bands due to the liquid show a constant separation of about 939 cm^{-1}. Comparing this with the frequencies observed in the spectrum of the vapour, it appears that this smaller value may be due to uncertainty in the location of the 0, 0 band exactly in the case of the liquid. The shift of the 0,0 band may be due to association of the molecules through the O—H group.

When the liquid is frozen and cooled to −180°C there is no appreciable change in the position of the 0, 0 band. The bands are a little sharper but still quite broad. This large width of the bands may be produced by the interaction of the permanent dipoles in the neighbouring molecules with the transition moment of the excited molecule. It is well known that large splittings are observed in some cases of substituted toluenes and dichlorobenzenes (Swamy, 1952, 1953; Sen, 1957). In the present case such splitting may be small and the large width of the individual bands may be responsible for the overlapping of the components and producing only a single broad band in place of its resolved components.

o-Bromoanisole

The absorption spectrum of *o*-bromoanisole in the vapour state consists of about 17 prominent bands. The strongest band on the long wavelength side at 35615 cm^{-1}, which persists at −20°C, has been taken as the 0, 0 band. The other bands have been interpreted on the basis of the fundamental frequencies 221, 358, 517, 632, 685, 744, 955, 1031 and 1233 cm^{-1} in the upper state and their combinations, and frequencies 189 cm^{-1} 233 cm^{-1} in the ground state. The acd frequencies 517, 632, 685, 744, 955, 1031 and 1233 cm^{-1} evidently correspond to the ground state frequencies 544, 659, 743, 792, 1023, 1122 and 1237 cm^{-1} observed in the infrared (Lecomte, 1938). No infrared data are available for frequencies lower

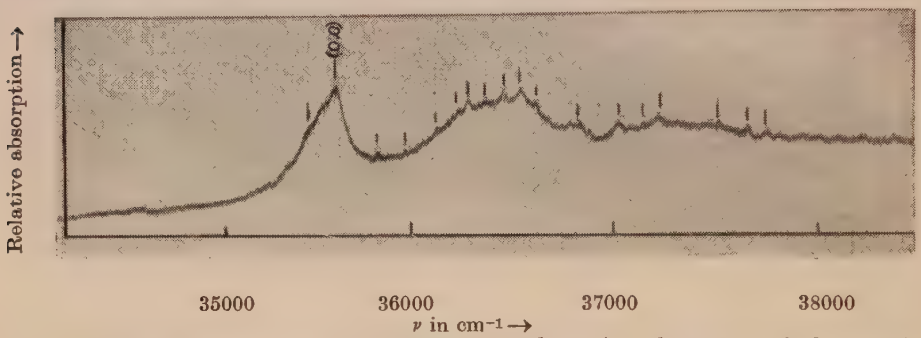

Fig. 3. Microphotometric record of the ultraviolet absorption of spectrum of *o*-bromoanisloe in the vapour state.

than 500 cm^{-1} and the Raman spectrum had not been studied by any previous worker, but the assignment of the frequencies 221 and 358 cm^{-1} to fundamental modes is probably justified. The frequency 358 cm^{-1} represents in all probability in the excited state one of the components of the e_g^+ mode (606 cm^{-1} in the ground state) of the benzene molecule which splits up into two totally symmetric components in the C_s point group. Further, similar band has also been observed in the case of other substituted anisoles (Suryanarayana and Rao, 1956). The frequency 221 cm^{-1} may be correlated to the observed ground state frequency 233 cm^{-1}, which again may represent an out of plane bending mode usually observed in the spectrum of disubstituted benzenes.

In the spectrum of the liquid only four broad bands are observed. Taking 35225 cm^{-1} as the position of the 0, 0 band, the other bands are separated from the 0,0 band by 221, 961 cm^{-1} and the first harmonic of 961 cm^{-1}. Thus it is seen that with the liquefaction of the vapour, the 0, 0 band is shifted by about 390 cm^{-1} towards red.

When the liquid is solidified and cooled to −180°C, no further resolution of the bands into components is observed. Taking 35139 cm^{-1} as the position of the 0, 0 band of the system, it is seen that the band system is further shifted towards longer wavelengths by about 86 cm^{-1} with the solidification of the liquid. The other bands of the solid represent excited state frequency 970 cm^{-1},

TABLE III

Ultraviolet sbsorption bands of *o*-bromoanisole in the vapour state

Wave No. (cm^{-1}) and Intensity	Assignment
35382 (w)	0 - 233
35438 (w)	0 − 189
35615 (vs)	0,0
35836 (w)	0 + 221
35973 (w)	0 + 358
36132 (mw)	0 + 517
36247 (mw)	0 + 632
36300 (s)	0 + 685
36359 (mw)	0 + 744
36468 (ms)	0 + 632 + 221
36570 (ms)	0 + 955
36646 (w)	0 + 1031
36848 (w)	0 + 1233
37039 (m)	0 + 685 + 744
37192 (w)	0 + 955 + 632
37246 (m)	0 + 955 + 685
37520 (m)	0 + 2 × 955
37620 (w)	0 + 2 × 685 + 632

TABLE IV

Ultraviolet absorption bands of *o*-bromoanisole in the liquid and solid states

Liquid at 32°C		Solid at −180°C	
Wave No. (cm^{-1}) and Intensity	Assignment	Wave No. (cm^{-1}) and Intensity	Assignment
35225 (s)	0,0	35139 (s)	0,0
35496 (w)	0 + 221		
36186 (s)	0 + 961	36109 (s)	0 + 970
37136 (s)	0 + 2 × 961	37081 (s)	0 + 2 × 970

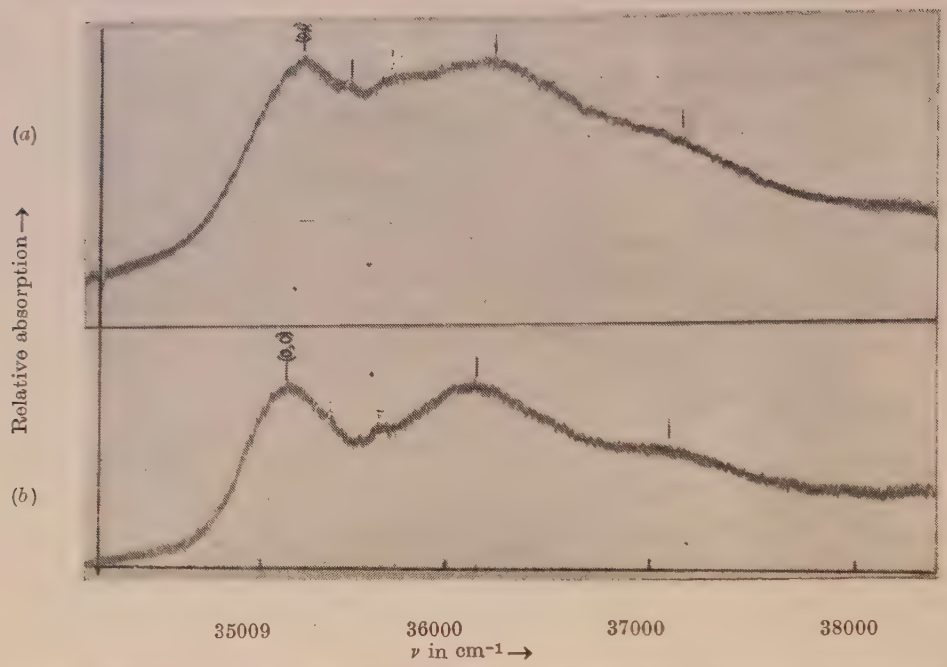

Fig. 4. Microphotometric records of the ultraviolet absorption spectra of *o*-bromoanisole. (a) Liquid at 32°C, (b) Solid at −180°C.

The disapperance of the other bands is due to broadening and consequent overlapping of the bands of the vapour, in the states of aggregation.

The bands are broad in the case of the liquid and the solid states. In the former case, both $v \rightarrow v$ transition and fluctuating intermolecular field may be responsible for the large width. Since both these causes disappear in the solid state, the persistence of the large width of the bands in this case may be due to unresolved components into which each band may have been split up by the interaction of the transition moment and permanent dipole of the surrounding molecules in the lattice.

ACKNOWLEDGMENT

The authors are grateful to Professor S. C. Sirkar, D.Sc., F.N.I., for his kind interest in the work and for valuable suggestions.

REFERENCES

Banerjee, S. B., 1956, *Ind. J. Phys.*, **30**, 106.
Kohlrausch, K. W. F. and Pongratz, A., 1935, *Monatsch. f. Chemie*, **65**, 199.
Lecomte, P. J., 1938, *J. de. Physique et Radium*, **9**, 13.
Ramasastri, C., 1951, *Proc. Nat. Inst. Sc.* (*Ind.*)., **17**, 349.
Sen, S. K., 1957, *Ind. J. Phys.*, **31**, 99.
Suryanarayana, V. and Rao, V. R., 1956, *Ind. J. Phys.*, **30**, 117.
Swamy, H. N., 1952, *Ind. J. Phys.*, **26**, 445.
,, ,, 1953, *Ind. J. Phys.*, **27**, 119.

BOOK REVIEW

MODERN GEOMETRICAL OPTICS—By Max Herzberger*. Pp 504+xii. Interscience Publishers, New York, London, 1958. Price $ 15.00

This book gives purely mathematical theories of image formation by optical systems. By representing the laws of reflection and refraction by an equation in which the vector product of two vectors in the object space is equated to a corresponding product in the image space, the problem of ray tracing has been reduced to that of solving equations involving vectors.

The book is divided into ten Parts, each part consisting of several Chapters. Part I of the book deals with the tracing of rays through optical systems and this can be done with the help of numerous formulae involving vectors and the necessary calculations can be made with the help of electronic computors. The terms "diapoint' and 'diamagnefication' have been introduced in this part and the properties of these points have been utilised in the succeeding parts. Part II deals with Gaussian Optics and its applications to different systems including thick lenses.

The general laws governing the passage of manifold of rays through optical systems have been discussed in Part III. As before, the vector equations have been given for these laws and the basic formulae of Hamilton and Lagrange have been discussed in this part. The formation of images by concentric systems has been discussed in Part IV and the vector formulae for the formation of images by rotation-symmetric systems including the discussions on image-error theory and limitations of optical image formation have been given in Part V.

The approximation theory of image formation in normal systems has been given in the different chapters of Part VI and the third and fifth-order image-error theories have been discussed in Part VII. In Chapter 31 of this Part formulae for the calculation of the characteristic functions for a combined system with the help of those for the parts of the systems have been derived.

Part VIII deals with interpolation theory of the optical image. The author himself has suggested an alternative method of solving the problem of image formation by complicated optical systems. In place of the actual ray tracing, help of some interpolation formulae is taken in this method. The analysis of spot diagrams is discussed in Chapter 33 in this Part.

Geometrical optics in inhomogeneous media is discussed in Part IX. Part X comprising four chapters, gives appendices dealing with 1) Vector analysis,

*The unusual delay in the publication of this review due two oversight is very much regretted. Editor.

2) Miscellaneous mathematical tools, 3) Numerical examples and 4) Historical remarks. A Bibliography is also given at the end.

The author himself has made remarkable contributions in this field and he has stated in the Preface that this book is the result of more than fourteen years' continuous labour. The tremendous amount of calculations required for the derivation of the numerous formulae and for their verification will show the amount of labour involved in the preparation of this volume which is a great treasure to opticians engaged in the design of high-precision optical systems. The book is especially useful to those workers in the field who have facilities for using electronic computors. It is also useful to post-graduate students interested in applied optics. The get-up is excellent.

S. C. S.

CONTENTS

Indian Journal of Physics Vol. 35, No. 4 April, 1961

PRINTED BY KALIPADA MUKHERJEE, EKA PRESS, 204/1, B. T. ROAD, CALCUTTA-35
PUBLISHED BY THE REGISTRAR, INDIAN ASSOCIATION FOR THE CULTIVATION OF SCIENCE
2 & 3, LADY WILLINGDON ROAD, CALCUTTA-32